Gas-Phase Spectroscopy and the Properties of Hydrogen-Bonded Dimers: HCN···HF as the Spectroscopic Prototype

A. C. LEGON*

Department of Chemistry, University of Exeter, Exeter EX4 4QD, United Kingdom

D. J. MILLEN*

Christopher Ingold Laboratories, Department of Chemistry, University College London, London WC1H 0AJ, United Kingdom

Contents

I. Introduction

The hydrogen bond was first postulated 65 years ago[1] and, because of the importance that it rapidly acquired

Figure 1. Diagrammatic representation of four normal modes involving the hydrogen bond in a linear dimer.

A. C. Legon has held the Chair of Physical Chemistry in the University of Exeter since 1984. He was born in Suffolk, England, in 1941 but was educated in London, first at the Coopers' Company School and then at University College London where he also conducted his doctoral research in the field of microwave spectroscopy. Subsequently, he was Turner and Newall Fellow (1968), Lecturer (1970), and finally Reader (1983) in the Chemistry Department at UCL. He spent the whole of 1980 on sabbatical leave in the late W. H. Flygare's laboratory at the University of Illinois (Champaign-Urbana). Professor Legon's research interests include the determination of geometries, potential energy functions, and electric charge distributions of small molecules (especially small cyclic molecules and hydrogen-bonded dimers B⋯HA) through rotational and vibrational spectroscopy.
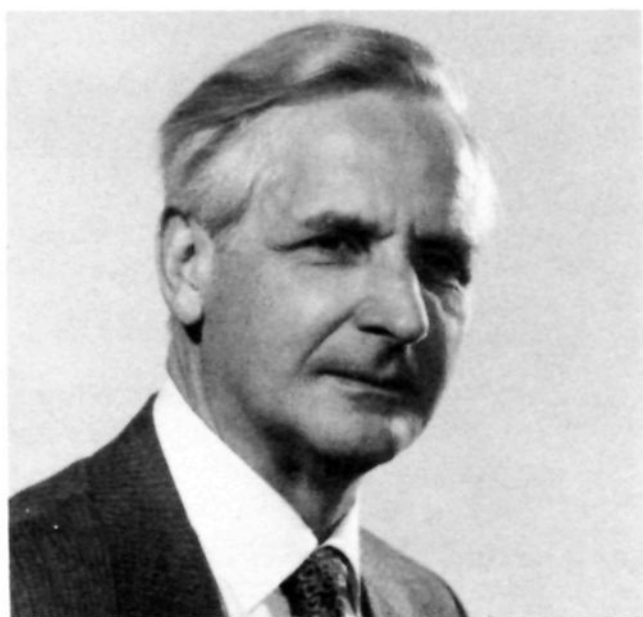
D. J. Millen received his B.Sc. and Ph.D. Degrees at University College London, the latter degree under the supervision of Dr. H. G. Poole and Sir Christopher Ingold. He held a Commonwealth Fund Fellowship at Harvard University in 1950–1951 where he worked with Professor E. Bright Wilson. He was appointed Professor of Chemistry in 1964 at University College London. In 1967 he was Nyholm Medallist and lecturer of the Royal Society of Chemistry and President of its Education Division for 1979–1981. His research interests in both infrared and microwave spectroscopy have now converged on a third research interest which he has had for many years on hydrogen-bonded dimers.

in both chemistry and biology, has been the subject of extensive research[2] ever since. Nevertheless, only recently has it been possible to investigate the intrinsic properties of the hydrogen bond. By intrinsic properties we mean those of the isolated dimer free from the lattice and solvent interactions that characterise the solid and solution phases. A range of techniques (for example, molecular beam electric resonance spectroscopy, pulsed-nozzle Fourier transform microwave spectroscopy, and infrared spectroscopy) has been used to observe the spectra of dimers under the required
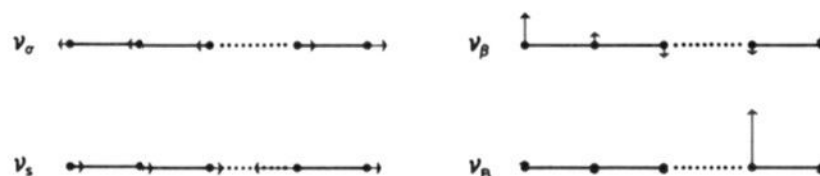
conditions of low pressure in the gas phase. Reviews of the spectroscopy of dimers using individual techniques have been published.[3-8] As a consequence of the spectroscopic activity, a wealth of information about a large number of hydrogen-bonded dimers is now available.

The purpose of the present review is to give an account of the origin and nature of both the infrared and microwave spectra and then to show how the properties of hydrogen-bonded dimers can be determined and interpreted. In particular, we shall elucidate the relationship between spectra, spectroscopic quantities, and dimer properties and, as will be shown below, this theme can be illustrated very conveniently from studies of a particular heterodimer involving a single hydrogen bond, supplemented by other examples as appropriate.

In this article we have used a nomenclature for hydrogen-bonded species which we believe is precise, convenient, and useful. Thus, we refer to HCN⋯HCN as a hydrogen-bonded *homodimer*, that is a species formed from *two* molecules of the *same* type. On the other hand, HCN⋯HF is a *heterodimer*, that is a species formed from *two* molecules of *different* types.

There are great advantages in working with heterodimers B⋯H–A. First, there is a wide range of such dimers and secondly B and HA can be chosen to satisfy the requirements of a particular investigation. Thus B and HA may be selected to provide, for simplicity, a linear dimer (e.g., HCN⋯HF) which facilitates a detailed spectroscopic study, or to provide a heterodimer which is advantageous for the determination of potential constants (e.g., $CH_3CN⋯HF$). Alternatively, a series of electron donors B may be chosen in order to investigate factors that determine the directional character of hydrogen bonds (e.g., dimers of the type O⋯H–F). Not least among considerations in the choice of B and HA for gaseous equilibrium studies are those which lead to a sufficiently strong bond to give a favourable equilibrium constant for formation of B⋯HA but not so strong an interaction that the volatility of the product is lost because of condensation of BH^+A^-. When sufficiently high resolution is available, as with techniques employing adiabatically expanded gas samples, it is possible to choose the heterodimer B⋯HA to allow conclusions about, for example, the electric charge redistribution or to allow the HA bond lengthening on dimer formation to be determined from the various types of nuclear hyperfine structure in the rotational spectrum.

In the earliest work, that involving low resolution infrared studies, it was the investigation of the heterodimers $(CH_3)_2O⋯HCl$ and HCN⋯HF that led to a detailed understanding of the vibrational spectra. This understanding greatly simplified the interpretation of the rotational spectra of heterodimers (observed later) such as HCN⋯HF, $CH_3CN⋯HF$, and $H_2O⋯HF$ because of the insight it gave into the rich vibrational satellite patterns which, it will be seen, are characteristic of such spectra. In fact, HCN⋯HF is the dimer that has been

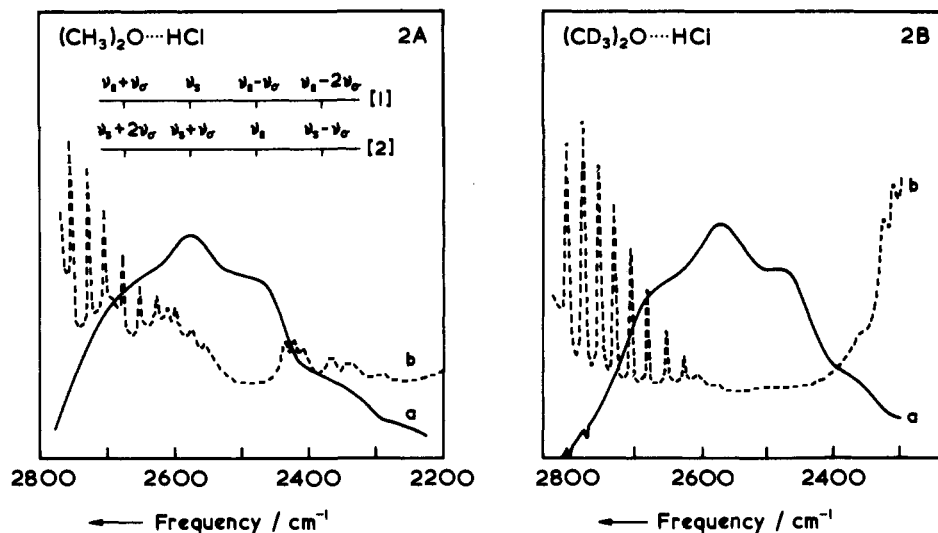**Figure 2.** A. (a) Spectrum of the dimer $(CH_3)_2O\cdots HCl$, (b) spectrum of the unmixed monomers. B. (a) Spectrum of the dimer $(CD_3)_2O\cdots HCl$, (b) spectrum of the unmixed monomers. Redrawn with permission from ref 9. Copyright 1965 The Chemical Society, London.

investigated in most detail not only by low resolution infrared and microwave spectroscopies but also by the higher resolution versions of these techniques. As a consequence, it has become possible to give an account of the spectroscopy of hydrogen-bonded dimers largely in terms of HCN$\cdots$HF and for the purposes of sequential development we will use in this article, where possible, this particular heterodimer to illustrate the wide range of properties of hydrogen-bonded dimers that can be determined spectroscopically. These properties will include the dimer geometry, the internal dynamics of the subunits, various aspects of the potential energy function, and changes in the electrical and geometrical properties of the monomers on formation of the hydrogen bond.

In section II, we present an account of the nature and analysis of the vibrational and rotational spectra of hydrogen-bonded dimers at various levels of resolution. Section III discusses how the spectroscopic quantities can be extracted from the observed spectra. Correspondingly, in section IV the properties of the dimer that can be determined from the spectroscopic quantities are illustrated, where possible, by reference to HCN$\cdots$HF. Finally, some generalizations about the hydrogen bond that have been made as a result of the type of spectroscopic studies reviewed are discussed.

II. Types of Spectroscopy Used in the Investigation of Hydrogen-Bonded Dimers

A. Low-Resolution Vibrational Spectroscopy

1. Nomenclature

One of the main conclusions from infrared spectroscopy of hydrogen-bonded dimers is that the observed low-resolution spectra can be interpreted satisfactorily in terms of vibrational modes closely associated with the hydrogen-bond. (Some of the internal modes of the monomers will, of course, exhibit detectable changes upon complex formation and can also provide information about the hydrogen bond.) In a linear dimer such as HCN$\cdots$HF, there are four hydrogen-bond

modes: the low-frequency stretching and bending modes ν_σ and ν_β, and higher frequency stretching and bending modes ν_S and ν_B, in the last two of which the motion is confined largely to the hydrogen atom (see Figure 1). The notation is directly applicable to symmetric rotor dimers, such as $CH_3CN\cdots HF$, while for asymmetric rotors with effective C_{2v} symmetry, such as $H_2O\cdots HF$, it is readily adapted by allowing the removal of the double degeneracy of each of ν_B and ν_β to give in- and out-of-plane modes $\nu_{B(i)}$, $\nu_{B(o)}$, $\nu_{\beta(i)}$, and $\nu_{\beta(o)}$. For dimers so far investigated by infrared spectroscopy, typical values for the wavenumbers of the $v = 1 \leftarrow 0$ transitions in these modes are as follows: ν_σ, $\sim$85–200 cm^{-1}; ν_S, $\sim$3000–4000 cm^{-1}; ν_β, $\sim$40–100 cm^{-1}; ν_B, $\sim$400–700 cm^{-1}.

2. Direct Observation of ν_S and ν_B in the Infrared Region

The earliest observations of the gas-phase vibrational spectra of simple hydrogen-bonded dimers having a single hydrogen bond were of broad bands associated with the high-frequency stretching modes ν_S. We show in Figure 2 the spectrum[9] of the HCl stretching region of the dimer $(CH_3)_2O\cdots HCl$, the spectral features of the monomers having been previously subtracted. The observation of essentially identical band structures for $(CH_3)_2O\cdots HCl$ and $(CD_3)_2O\cdots HCl$, as shown in Figure 2a and 2b, served to exclude Fermi resonance as a cause of band breadth and structure, an interpretation that had been prevalent up to that time. The origin of the large breadth of the observed bands has been much discussed and its interpretation is considered in section IIA3 below. The corresponding feature in our prototype dimer HCN$\cdots$HF is in fact less well-defined, and hence we refer here to the dimethyl ether–HCl complex, the key dimer in establishing the assignment of the ν_S-band structure, although such effects have now been observed for many complexes including HCN$\cdots$HF.

The mode ν_B, on the other hand, has been less frequently observed, but a good illustration of its nature is presented by the example of HCN$\cdots$HF. Thus, in Figure 3 the region of the $\nu_B = 1 \leftarrow 0$ transition of HCN$\cdots$HF is shown.[10] The obvious structure on this
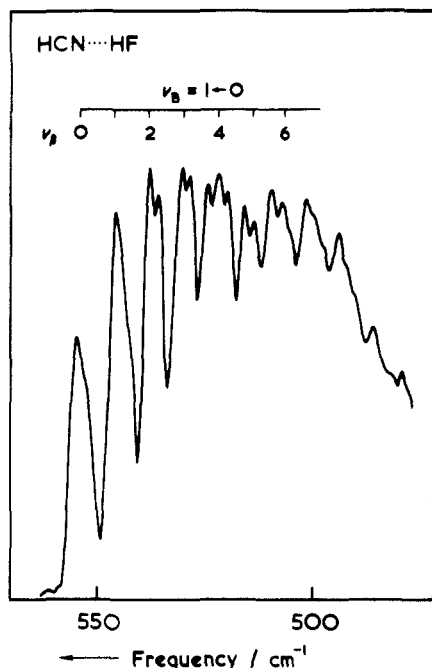
Figure 3. A sequence in the low-frequency bending mode ν_β appearing on the ν_B band in the infrared spectrum of HCN$\cdots$HF. Redrawn with permission from ref 10. Copyright 1971 Royal Society (London).

band will receive interpretation in section IIA3.

3. ν_σ Progressions Associated with ν_S and Sequences in ν_β Associated with ν_B

Although the structure evident within the ν_S band shown in Figure 2a and 2b has been the subject of extensive discussion, there is now a generally accepted interpretation. The structure arises, in fact, from a progression in the low-frequency stretching mode ν_σ based on the high-frequency stretching mode ν_S. Two possible assignments of this progression that have been made are given in Figure 2. The most recent evidence[11] indicates that assignment 1 is to be preferred. Investigations show that the first overtone bands $\nu_S = 2 \leftarrow 0$ for $R_2O\cdots HF$ have similar structures with sub-bands at $2\nu_S - \nu_\sigma$, $2\nu_S$ and $2\nu_S + \nu_\sigma$, etc. and lead to values for important anharmonicity constants.[12] For HCN$\cdots$HF, an analogous structure has been observed for the fundamental and assigned unambiguously[10,13] as $\nu_S - \nu_\sigma$, ν_S, and $\nu_S + \nu_\sigma$.

The structure seen on the $\nu_B = 1 \leftarrow 0$ band of HCN$\cdots$HF in Figure 3 has an analogous interpretation to that associated with ν_S but involving the two bending modes ν_B and ν_β. Thus, each component in the structure corresponds to a transition $\nu_\beta\nu_\beta + \nu_B \leftarrow \nu_\beta\nu_\beta$ beginning at $\nu_\beta = 0$ on the right-hand side in Figure 3 and increasing in steps of one in ν_β to the left, thereby forming a sequence of hot bands in ν_β and allowing the evaluation of anharmonicity constants.[10] The assignment of quantum numbers in this sequence is included in Figure 3.

4. Direct Observation of ν_σ in the Far Infrared Region

The difference between consecutive features of the band structure in the $\nu_S + \nu_\sigma$ progression (see Figure 2) leads to an approximate value for the vibrational separation $\nu_\sigma = 1 \leftarrow 0$ and has allowed identification of this transition in the far-infrared region in a few cases. Thus
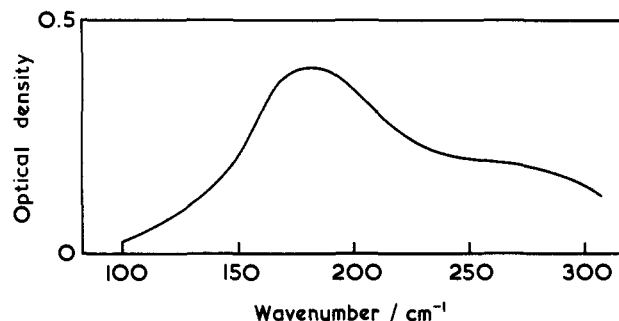
Figure 4. Far infrared spectrum of the dimer $Me_2O\cdots HF$. The monomer spectra have been subtracted from the spectrum of the mixture. Redrawn with permission from ref 16. Copyright 1971 Royal Society (London).

for $(CH_3)_2O\cdots HCl$ the value approximately 100 cm^{-1} is obtained[9] from sum and difference bands in ν_S while the far infrared measurements[14] give 118 ± 1 cm^{-1}. For $(CH_3)_2O\cdots HF$, the approximate value obtained[15] from the ν_σ progression on ν_S is 170 cm^{-1} while the $\nu_\sigma = 1 \leftarrow 0$ transition itself is observed[16] at 185 cm^{-1}, as shown in Figure 4. No direct observation has been made for $\nu_\sigma = 1 \leftarrow 0$ in HCN$\cdots$HF but a value of 155 cm^{-1} has been determined[10] from the ν_σ progression on ν_S.

B. Low-Resolution Rotational Spectroscopy

1. An Early Broadband Rotational Spectrum

The first rotational spectrum of a heteromimer involving a single hydrogen bond was that of the symmetric top species $CH_3CN\cdots HF$ observed at rather high partial pressures of the two components using a Hewlett Packard 8460A Stark modulation spectrometer and an equilibrium gas mixture.[17,18] It consisted of a set of equally spaced, very broad bands which do not appear in the spectra of each of the separate components. One such band, the $J = 4 \leftarrow 3$ transition, is shown in Figure 5 along with a trace of the same spectral region for each of the components. The bands are equispaced as expected for a symmetric rotor and lead directly to a value for B.

2. The Rotational Spectrum under Increased Resolution

The broad band seen in Figure 5 is the envelope of vibrational satellites, K-sub band structure and nuclear hyperfine components. When the partial pressures of the two components are reduced[9] each broad band in the rotational spectrum of $CH_3CN\cdots HF$ referred to above and shown in Figure 5 resolves into a large number of components, as illustrated for the $J = 8 \leftarrow 7$ transition in Figure 6. Each resolved component now corresponds to the same rotational transition ($J = 8 \leftarrow 7$) but in a different vibrational state.[18] The existence of a strong vibrational satellite progression, which must be associated with the lowest energy mode of the molecule (that is the doubly degenerate hydrogen-bond bending mode ν_β, see Figure 1), is clear but the identity of the ground-state transition is not immediately obvious. However the indicated progression is almost equally spaced, requiring that the first member of the series at 29 645.2 MHz be assigned to the vibrational ground state and the remainder to states with successive quanta of ν_β excited, as labelled in Figure 6. The unusual fact that the strongest transition in a satellite

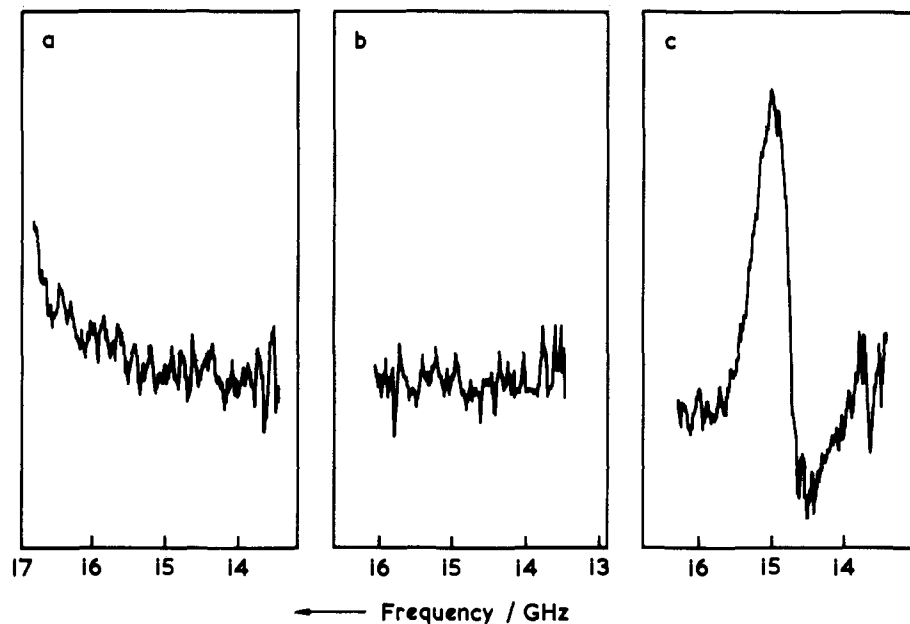**Figure 5.** Detection of the heterodimer formed between methyl cyanide and hydrogen fluoride by means of its gas-phase rotational spectrum. Rotational spectra of (a) CH_3CN flowing through cell at pressure ca. 0.5 torr; (b) HF flowing through cell at pressure ca. 0.8 torr; (c) approximately equal partial pressures of CH_3CN and HF flowing through cell at total pressure ca. 0.9 torr. Redrawn with permission from ref 18. Copyright 1980 Royal Society (London).
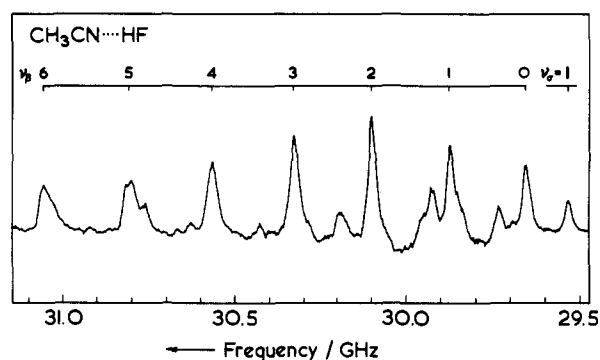
Figure 6. The ground-state $J = 8 \leftarrow 7$ rotational transition and its vibrational satellites for $CH_3CN\cdots HF$ under moderate resolution. (Partial pressures of components are approximately equal and the total pressure is ca. 0.12 Torr.) Redrawn with permission from ref 18. Copyright 1980 Royal Society (London).

progression is not associated with the ground state has its origin in the double degeneracy of the mode ν_β and will be discussed further in section IIIA2. To the low frequency of the ground-state transition is the satellite associated with the $v_\sigma = 1$ state. A progression in ν_β but based on $v_\sigma = 1$ is clearly evident.

At even lower pressures and, therefore, higher resolution, the vibrational ground state transition itself is shown to consist of several components.[18] This substructure corresponds to the $K \leftarrow K$ components of the $J + 1 \leftarrow J$ transition, as illustrated for the $J = 8 \leftarrow 7$ spectrum in Figure 7. The stick diagram indicates the positions of the K substructure calculated on the basis of $D_{JK} = 67$ kHz used in the familiar frequency expression

$$\nu = 2B_0(J + 1) - 4D_J(J + 1)^3 - 2D_{JK}(J + 1)K^2 \qquad (1)$$

for centrifugal distortion in a symmetric rotor molecule. When the dimer is a linear species like $HCN\cdots HF$, the double degeneracy of mode ν_β is lifted by l-type doubling effects with the consequence that each member of the ν_β progression has a l-substructure (but of course
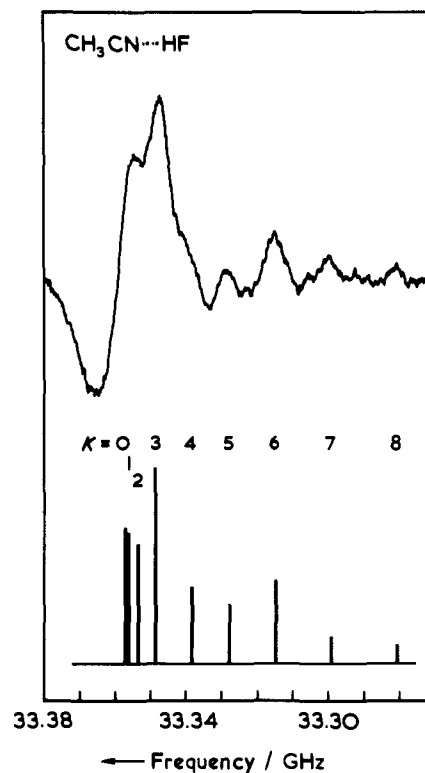
Figure 7. The ground-state $J = 9 \leftarrow 8$ rotational transition of $CH_3CN\cdots HF$ under higher resolution showing the K substructure.

no K-substructure) as indicated for the ν_β progression in the $J = 5 \leftarrow 4$ transition of $HC^{14}N\cdots HF$, in Figure 8. This spectrum, like those in Figures 5, 6, and 7, has been observed by Stark modulation microwave spectroscopy.[19] Again, the satellite corresponding to $v_\sigma = 1$ falls to low frequency of the ground-state transition and is the origin of a second progression (ν_β, $v_\sigma = 1$) in ν_β.

For asymmetric rotors such as $H_2O\cdots HF$, the double degeneracy of ν_β is lifted, yielding the modes $\nu_{\beta(i)}$ and $\nu_{\beta(o)}$. The vibrational satellite pattern in the rotational
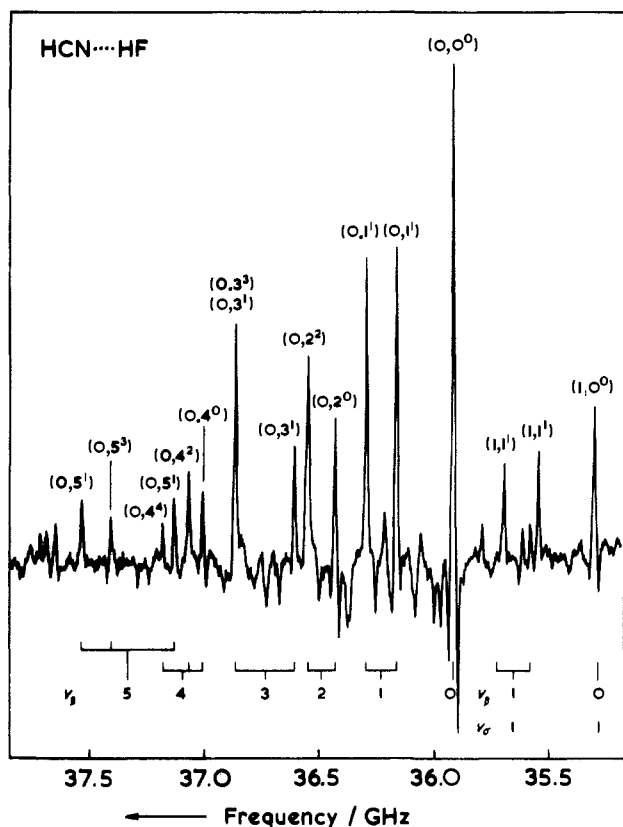
Figure 8. The $J = 5 \leftarrow 4$ transition for HCN···HF showing progression of satellite transitions for the mode ν_β. Redrawn with permission from ref 135. Copyright 1982 The Royal Society of Chemistry.

spectrum becomes correspondingly more complicated but a detailed analysis[20] leads to a quantitative form of the double minimum potential energy function which governs the mode $\nu_{\beta(o)}$. When the asymmetric rotor molecule is a homodimer, such as $(H_2O)_2$ or $(HF)_2$, the equivalence of the subunits introduces the possibility of permutation inversion and, associated with this, complicated spectra which have been analysed by the MBERS method in some elegant investigations.[21,22]

3. Observation of the Stark Effect

An advantage of using a Stark-modulated microwave spectrometer to record rotational spectra is that the Stark effect of a transition is automatically obtained, and conveniently the Stark components are displayed simultaneously with the zero field transition but 180° out of phase. This effect is clearly evident in the downward pointing components associated with the vibrational ground-state $J = 5 \leftarrow 4$ transition of HC-N···HF as shown in Figure 8, but is more clearly demonstrated in the $J = 3 \leftarrow 2$ ground-state transition shown in Figure 9 where the M_J values associated with the $M_J \leftarrow M_J$ Stark components (the only type allowed by the spectrometer configuration) are indicated.

C. High-Resolution Rotational Spectroscopy of Supersonically Expanded Gas Mixtures

1. Unambiguous Identification of Ground-State Rotational Spectra of Dimers

The rotational spectra shown in Figures 5–9 inclusive were obtained using conventional Stark-modulation microwave spectroscopy[19] of an equilibrium gas mixture
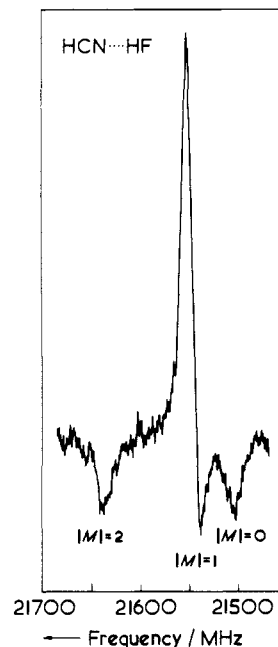
Figure 9. Stark effect for the $J = 3 \leftarrow 2$ transition of HCN···HF.

of the two components at temperatures ≈ 200 K. In fact, the transitions carry a hyperfine structure that arises from ^{14}N nuclear quadrupole and H,F nuclear spin–nuclear spin coupling but, for the conditions under which the spectra were recorded, this was not resolved. Attempts to cool the gas mixture and lower the pressure in order to improve the resolution are unsuccessful because the loss of vapour pressure defeats the gain in signal brought about by the improved equilibrium constant. It is necessary effectively to cool the gas mixture but at the same time avoid condensation. This result can be achieved by adiabatic expansion of a gas mixture of the components B and HA seeded in argon through a nozzle. The rotational spectrum of the expanded gas, which is rich in the required species B···HA and of low effective temperature, is detected subsequently. Two techniques using such a supersonically expanded gas are available: pulsed-nozzle, Fourier-transform microwave spectroscopy[23] and molecular-beam, electric-resonance spectroscopy[22] (see section IIE).

Both techniques employing supersonic expansion of the mixture of B and HA enjoy two important advantages over Stark-modulation microwave spectroscopy. The first of these is a very high resolution which will be illustrated in section IIC2. The second also arises because of the low effective temperature of the expanded gas. This ensures that, in most cases, only the ground state rotational spectrum is observed and can for certain dimers provide the only method of identifying the vibrational ground-state spectrum. The dimer HCN···HCN provides an example where the identification of the ground state transition in the Stark-modulation spectrum was a severe problem.[24,25] In this case each rotational $J + 1 \leftarrow J$ transition exhibits at least thirty vibrational satellites and, because the rotational constant $2B$ is relatively small, the later members of the satellite series encroach on the region of the $J + 2 \leftarrow J + 1$ transition. Moreover, although vibrational satellites associated with low-frequency, doubly degenerate bending modes are readily modulated and therefore easily detected when investigated by Stark
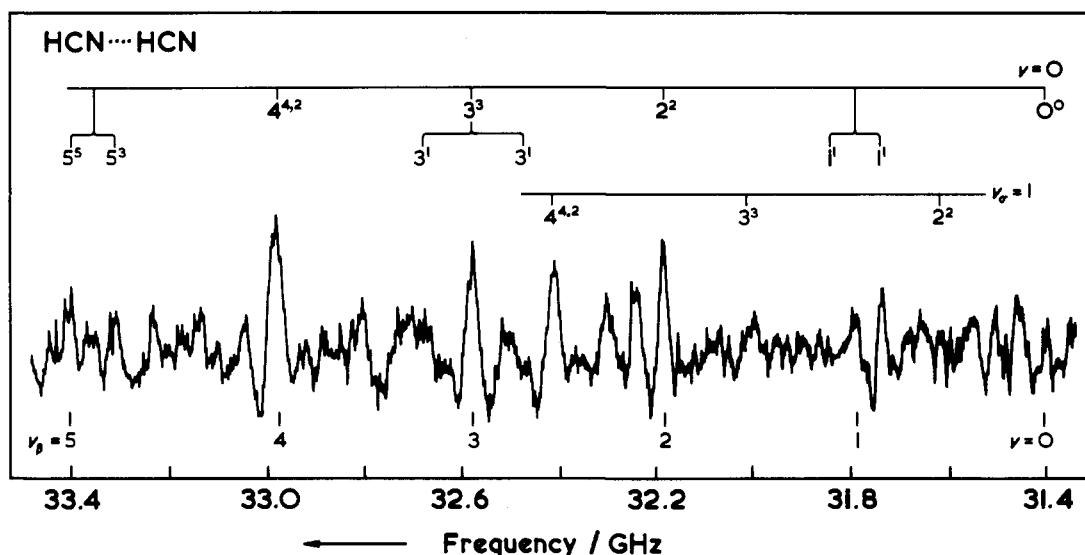
Figure 10. Vibrational satellites of the $J = 9 \leftarrow 8$ transition of $(HC^{14}N)_2$ recorded at $E \approx 200$ V cm^{-1}, $p \approx 65$ Pa, $T \approx 190$ K. Redrawn with permission from ref 25. Copyright 1985 Royal Society (London).

modulation spectroscopy, the vibrational ground-state transition is difficult to observe because it exhibits only a second-order Stark effect. Once the ground-state transitions of this linear homodimer had been identified unambiguously by pulsed-nozzle, FT microwave spectroscopy[26] it was possible[25] to assign the vibrational satellite pattern in an analogous way to that described for HCN···HF. The region of the $J = 9 \leftarrow 8$ transition in the Stark modulation spectrum of HCN···HCN is shown in Figure 10. Under the indicated conditions, the ground-state transition is insufficiently modulated but the ν_β vibrational satellites are clearly observed to high frequency of the position of the $v = 0$ transition as calculated from the results of the pulsed-nozzle investigation. Only after the ground-state transition had been located in this way was it possible to assign the quantum numbers to the vibrational satellites shown in Figure 10.

2. Resolution of Nuclear Quadrupole- and Nuclear Spin–Nuclear Spin Hyperfine Splittings

The first advantage, alluded to above, of employing supersonic expansion of a seeded gas mixture of B and HA in argon is the high resolution resulting from the absence of pressure broadening in the collisionless expansion. The high resolution in the presence of high sensitivity that characterises the pulsed-nozzle, FT method can be illustrated[27] by the example of the $J = 1 \leftarrow 0$ transition of the isotopic species HC^{14}N···HF, which is shown in Figure 11. This transition consists of a gross triplet at frequencies approximately 7181.25, 7182.5, and 7184.35 MHz corresponding to the three ^{14}N-nitrogen nuclear quadrupole components. Each component of the triplet has a substructure which arises from H,F nuclear spin–nuclear spin coupling. It should be noted that all of the components shown in Figure 11 would fall within a single line width of the spectrum displayed in Figure 8. On the other hand, none of the vibrational satellites shown in Figure 8 is observed in the pulsed-nozzle experiment because of the low effective temperature. As explained in section IIE1 it is a great advantage of Stark modulation spectroscopy of gaseous mixtures that it allows the potential energy functions of hydrogen-bonded dimers to be probed
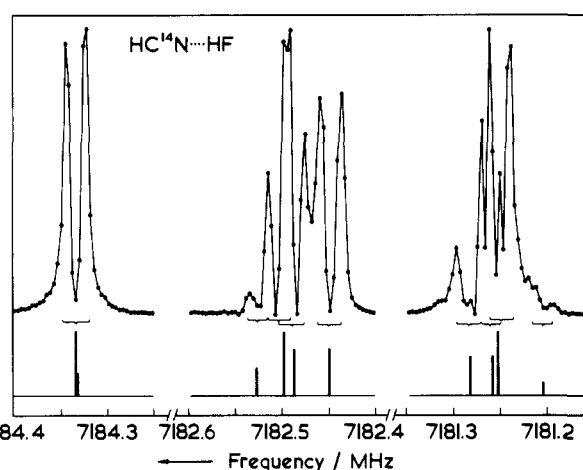
Figure 11. A composite diagram of the frequency domain recordings of each of the three groups of hyperfine components in the $J = 1 \leftarrow 0$ transition of HC^{14}N···HF. The absolute frequency scale is indicated on the abscissa to show the different magnitudes of the ^{14}N nuclear quadrupole splitting (gross structure) and the H,F spin–spin splitting (fine structure). The stick diagram shows the calculated positions of the components. The doubling indicated by the braces is an instrumental (Doppler) effect. Redrawn with permission from ref 27. Copyright 1985 Royal Society (London).

through the observation of vibrational satellites. The results of Stark-modulation and pulsed-nozzle, FT microwave spectroscopies are in this sense complementary.

We can demonstrate[27] that the gross triplet in Figure 11 arises from ^{14}N-nuclear quadrupole coupling by considering the $J = 1 \leftarrow 0$ transition of the isotopic species HC^{15}N···HF which is recorded in Figure 12. The spectrum is now greatly simplified (^{15}N has a nuclear quadrupole moment of zero) and only the four components arising from H,F nuclear spin–nuclear spin coupling remain. Another illustration[27] of the high resolution possible by pulsed-nozzle, FT microwave spectroscopy is given by Figure 13 in which we show the $J = 1 \leftarrow 0$ transition of HC^{15}N···DF. In this case, the hyperfine structure, which is spread over only 200 kHz, arises mainly from D-nuclear quadrupole coupling but with a small contribution from D,F nuclear spin–nuclear spin splitting.
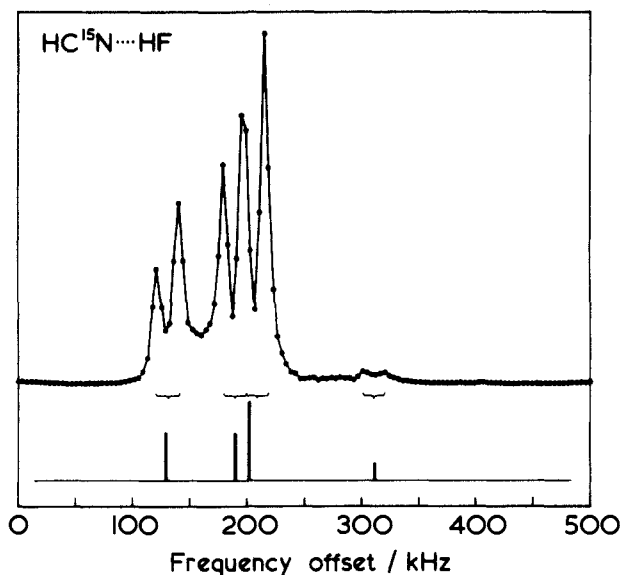
Figure 12. Recording of the $J = 1 \leftarrow 0$ transition of $HC^{15}N\cdots HF$. Frequencies are offset at a rate of 3.906 25 kHz per point from the polarizing frequency 7146.9558 MHz. The stick diagram shows the calculated positions of the hyperfine components. The doubling indicated by the braces is an instrumental (Doppler) effect. Redrawn with permission from ref 27. Copyright 1985 Royal Society (London).
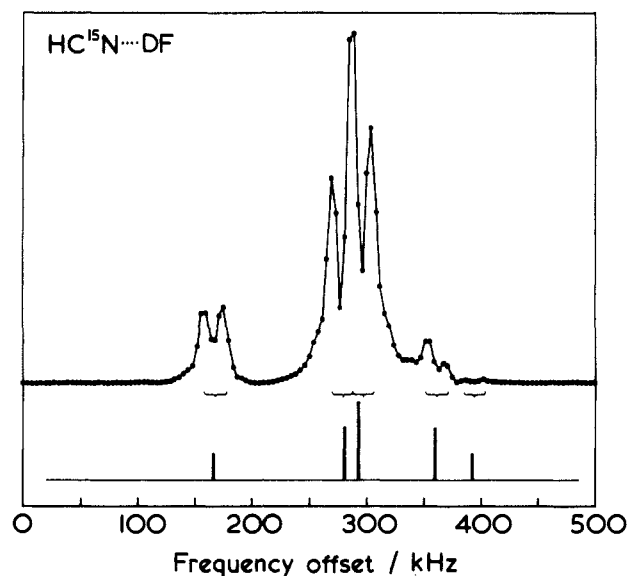
Figure 13. Recording of the $J = 1 \leftarrow 0$ transition of $HC^{15}N\cdots DF$. Frequencies are offset at a rate of 3.906 25 kHz per point from the polarizing frequency 7102.6923 MHz. The stick diagram shows the calculated positions of the hyperfine components. The doubling indicated by the braces is an instrumental (Doppler) effect. Redrawn with permission from ref 27. Copyright 1985 Royal Society (London).

D. High-Resolution Vibration–Rotation Spectroscopy

1. Resolution of Rotational Fine Structure in $v_S = 1 \leftarrow 0$ Vibrational Transitions

If we focus attention on the subband associated with $v_\sigma = 0$ in the $v_S + v_\sigma v_\sigma \leftarrow v_\sigma v_\sigma$ region of the infrared spectrum of $HCN\cdots HF$ referred to in section IIA3 and increase the resolution,[10] the result is shown in Figure 14. We note a substructure which has been assigned by Thomas[10] as a sequence of hot bands in the low-frequency bending mode v_β. Thus, each component in the substructure consists of a transition of the type v_S
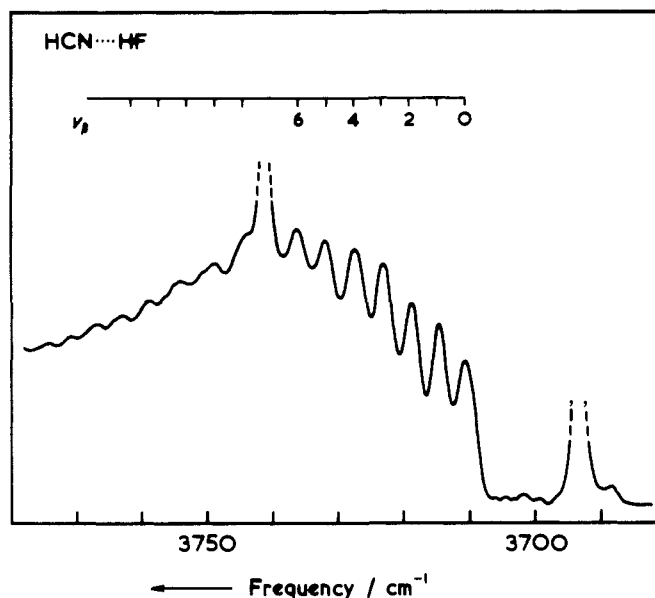
Figure 14. Substructure associated with v_S for $HCN\cdots HF$. Values of v_β indicate assignment as a sequence of hot bands in the low-frequency bending mode v_β. Redrawn with permission from ref 10. Copyright 1971 Royal Society (London).
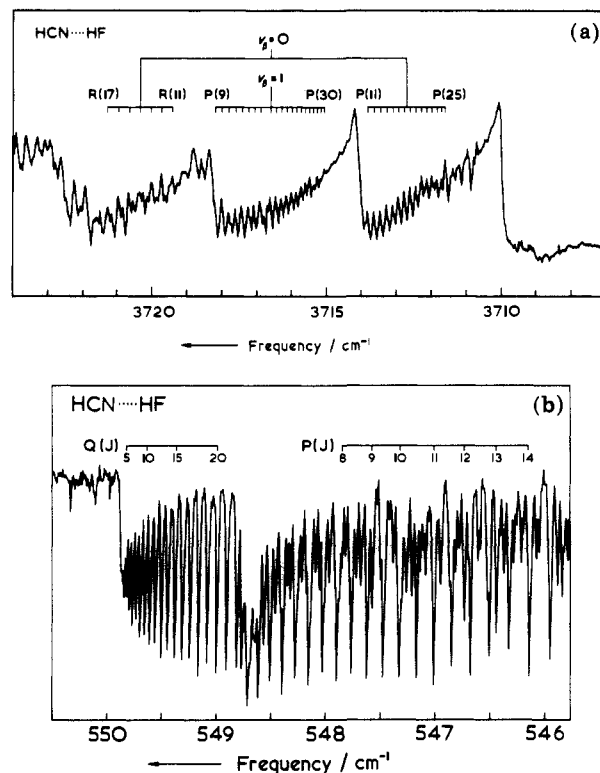
Figure 15. (a) Part of the $v_\beta v_\beta + v_S \leftarrow v_\beta v_\beta$ high-resolution infrared spectrum of $HCN\cdots HF$ illustrating the partially resolved $P(J)$ and $R(J)$ branch transitions associated with $v_\beta = 0$ and $v_\beta = 1$ states. Total pressure 0.5 torr, temperature 213 K and 96 m effective path length. Redrawn with permission from ref 13a. Copyright 1983 American Institute of Physics. (b) Part of the $v_\beta v_\beta + v_B \leftarrow v_\beta v_\beta$ high resolution infrared spectrum of $HCN\cdots HF$ illustrating $P(J)$ and $Q(J)$ branch transitions associated with the $v_\beta = 0$ state. Redrawn with permission from ref 13b.

+ $v_\beta v_\beta \leftarrow v_\beta v_\beta$, that is the analogue of the sequence associated with the $v_B = 1 \leftarrow 0$ transition shown in Figure 3.

If we now further focus our attention on the first two members (i.e., $v_\beta = 0$ and $v_\beta = 1$) of the sequence shown in Figure 14 and again increase the resolution the result

is that obtained by Bevan et al.[13(a)] which is displayed in Figure 15(a). The spectrum in Figure 15(a) is annotated by the assignment of rotational fine structure for each $\nu_S + \nu_\beta\nu_\beta \leftarrow \nu_\beta\nu_\beta$ transition, where $\nu_\beta = 0$ and 1, and this shows clearly that the substructure apparent in Figure 14 has its origin in a P-branch bandhead in each case, as originally proposed by Thomas.[10] The basis of the proposal was that, because of the Sheppard effect,[28] the hydrogen bond is shortened by Δr in the $\nu_S = 1$ state by comparison with the $\nu_S = 0$ state. The result is that $B_0 - B_1$ is negative and as a consequence each P-branch converges to form a sharp bandhead. Indeed, the high resolution study of ν_S in HCN···HF provides the first direct experimental evidence of the Sheppard effect and leads to the value $\Delta r = 0.034$ Å.

An analogous investigation[29] of the homodimer $(HF)_2$ has been made in which a wealth of rotational fine structure associated with ν_S has been analyzed, taking into account the inversion motions arising from the equivalence of the HF subunits.

2. Resolution of Rotational Fine Structure in $v_B = 1 \leftarrow 0$ Vibrational Transitions

The ν_B band of HCN···HF has been recently recorded under very high resolution by Bevan et al.[13(b)] and is shown in Figure 15(b). The band consists of the P-, Q-, and R-branches expected for a $\Pi \leftarrow \Sigma$ bending band of a linear molecule. The vibrational change in the B rotational constant is anomalously large and negative, and the R-branch forms a sharp and distinctive head around $J = 50$. In fact, Thomas,[13(a)] lacking the resolution available in this study, understandably mistook this R-branch for a Q-branch. The fundamental band is accompanied by a maze of hot-band transitions which fortunately are displaced to low frequency and which also contain R-branch as well as Q-branch heads. Analysis of the rotational fine structure of the ν_B band leads to a very accurate rotational constant B_B, centrifugal distortion constant $D_J{}^B$ and the l-type doubling constant q_B.

E. Summary of Experimental Methods Used To Observe Spectra

We summarize below the methods used to record the spectra shown in Figures 2–15. More detailed descriptions can be obtained from the indicated references.

Low-resolution infrared spectra have been observed with conventional spectrometers and, where appropriate, long-path gas cells.[9,10,15] On the other hand, the high resolution infrared spectra were investigated either by means of tunable, color-center or frequency-difference lasers and very long-path, White cells which could be cooled to low temperature[13a,29] or by means of a FTIR spectrometer and a multipass cell.[13b]

The low-resolution rotational spectra were recorded with a Hewlett-Packard 8460A 33 kHz Stark-modulated microwave spectrometer employing phase-sensitive detection.[19] The gold-plated absorption cell of this spectrometer proved to be a significant advantage when working with mixtures containing hydrogen fluoride. The control of the temperature of the microwave absorption cell was a crucial operation in these experiments because, on the one hand, as low a temperature as possible was required to favor the dimer but, on the

other hand, condensation of the mixture placed a lower limit on the working temperature. Temperatures in the range −70 to −30 °C were commonly used and were achieved by cooling with liquid nitrogen. Each half of the absorption cell was enclosed by an insulated jacket into which liquid nitrogen could be pumped, at a rate controlled by a sensing platinum resistance thermometer, from a Cryoson pressurized dewar. The liquid nitrogen was delivered at eight points onto a baffle plate above the absorption cell via a branching system of polythene pipes insulated with foam rubber.

The high-resolution rotational spectra discussed above were detected by means of the pulsed-nozzle, Fourier-transform microwave technique.[4,23] This involves Fourier-transform microwave spectroscopy of a pulse of gas mixture (B and HA diluted in, say, argon) expanded supersonically from a nozzle into an evacuated Fabry–Perot cavity. The microwave pulse induces a macroscopic polarization in the gas when it is in collisionless expansion between the Fabry–Perot mirrors. It is required that the half-life, T_2, for the decay of the macroscopic polarization is much greater than that (τ_c) for the decay of the microwave pulse within the Fabry–Perot cavity. Accordingly, when the polarized dimers in the cold gas $(T \approx 5$ K$)$ begin to emit at some rotational transition frequency and the detector is opened, the microwave pulse has dissipated and only the molecular emission survives to be detected. Details of the theory and operation of this technique have been described.[4,23]

Some of the results from high-resolution rotational spectra referred to below have been determined by molecular-beam electron resonance spectroscopy (MBERS). The technique has been reviewed a number of times.[8,30] Basically, inhomogeneous electric fields are used to deflect molecules, through the Stark effect, from beams of the supersonically expanded mixture of B and HA in argon. This effect depends strongly on the rotational state of the dimer and hence electric dipole transitions are detected by altering the trajectories of the dimers that have suffered a rotational transition. As a consequence, only molecules that have certain trajectories are allowed to reach the detector which is usually a mass spectrometer. The number of dimers reaching the detector as a function of the radiation frequency yield the required spectrum.

The techniques discussed above for the detection of low- and high-resolution rotational spectra are complementary. Although equilibrium rotational spectroscopy is restricted mainly to moderately strongly hydrogen-bonded dimers and has moderate resolution, it has the significant advantage that rotational spectra are obtained in vibrationally excited states of the low-lying hydrogen-bond modes as well as in the vibrational ground state. Vibrational satellites are important because of the information they contain about the hydrogen bond potential energy function. The pulsed-nozzle, Fourier-transform and MBERS methods have, on the other hand, a very high sensitivity for molecular dimers and a high resolution because of the low effective temperature of the gas pulse and because the emission/absorption of radiation occurs while the gas is in collisionless expansion. Very weakly bound molecular dimers can be investigated with these instruments. A concomitant disadvantage of the low effective tem-

TABLE I. Vibrational Energy Separations (cm⁻¹) in HCN• • •HF and CH₃CN• • •HF

vibrational spacing	infrared	microwave relative intensity	l-type doubling	centrifugal distortion
HCN···HF				
$\nu_S = 1 \leftarrow 0$	3716.20 ± 0.01	–	–	–
$\nu_\sigma = 1 \leftarrow 0$	155 ± 10	197 ± 15	–	163
$\nu_B = 1 \leftarrow 0$	555 ± 3	–	–	–
$\nu_\beta = 1 \leftarrow 0$	70 ± 24	91 ± 20	72	–
ref	10	19	60	27
CH₃CN···HF				
$\nu_S = 1 \leftarrow 0$	3627 ± 2	–	–	–
$\nu_\sigma = 1 \leftarrow 0$	168 ± 3	181 ± 20	–	158 ± 2
$\nu_B = 1 \leftarrow 0$	620 ± 3	–	–	–
$\nu_\beta = 1 \leftarrow 0$	40 ± 14	45 ± 15	–	–
ref	10	18	–	56

TABLE II. Rotational and Centrifugal Distortion Constants for HCN• • •HF

isotopic species	B_0, MHz	D_J, kHz
HC¹⁵N···HF	3573.5874 (2)	6.97 (2)
HC¹⁵N···DF	3551.5110	6.83
HC¹⁴N···HF	3591.1552	6.99
HC¹⁴N···DF	3569.6576	6.86
DC¹⁵N···HF	3360.3549	5.85
DC¹⁵N···DF	3338.0824	5.81
DC¹⁴N···DF	3351.87 (4)	5.5 (8)
H¹³C¹⁴N···HF	3496.13 (6)	6.6 (assumed)

perature is, however, that spectra in the vibrational ground state only are observed. The equilibrium and MBERS methods, through the Stark effect, readily furnish electric dipole moments of dimers, while the high resolution of the pulsed-nozzle, Fourier-transform, and MBERS methods allow the investigation of nuclear quadrupole and nuclear spin–nuclear spin coupling effects.

III. Determination of Spectroscopic Quantities from Observed Spectra

A. Introduction

The spectra that have been used illustratively in the preceding section contain a wealth of information about the dimers from which they are derived. We begin by discussing the spectroscopic quantities that can be extracted from spectra of the types shown and these will then be used in section IV to show how the *molecular* properties of the dimers can be determined from them.

B. Vibrational Spacings in ν_S, ν_σ, ν_B, and ν_β

1. Determination from Infrared Spectroscopy

We refer to the example of HCN···HF. For this heterodimer, ν_S and ν_B have been determined directly[10] from the origin of the $\nu_\beta\nu_\beta + \nu_S \leftarrow \nu_\beta\nu_\beta$ sequence shown in Figure 14 and the origin of the $\nu_\beta\nu_\beta + \nu_B \leftarrow \nu_\beta\nu_\beta$ sequence shown in Figure 3, respectively. On the other hand, ν_σ and ν_β for HCN···HF have not, so far, been observed directly but both can be obtained indirectly. The wavenumber of the former follows from the difference of ν_S and $\nu_S - \nu_\sigma$ as observed by Thomas.[10] The wavenumber of the latter is obtained from the intensity variation in the $\nu_\beta\nu_\beta + \nu_B \leftarrow \nu_\beta\nu_\beta$ sequence,[10] for which the relative intensities are given by

$$I(\upsilon_\beta)/I(0) = (\upsilon_\beta + 1) \exp(-hc\upsilon_\beta\nu_\beta/kT) \qquad (2)$$

under the assumption that the electric dipole transition moment is negligibly changed on excitation of ν_β. The vibrational separations obtained for ν_S, ν_σ, ν_B, and ν_β from infrared spectroscopy are collected together in Table I.

2. Determination of ν_σ and ν_β from Rotational Spectroscopy

It is convenient initially to refer here to the example of CH₃CN···HF[18] instead of the closely related HCN· ··HF because of complications imposed by resolved l-

type doubling effects among the vibrational satellites in the rotational spectrum of the latter.[19] The extended vibrational satellite series associated with the $J = 8 \leftarrow 7$ transition of the symmetric top CH₃CN···HF has been illustrated in Figure 6. The intensity of a member of the ν_β progression relative to that of the ground state is also given[18] by eq 2, which thereby draws attention to the close relationship between the sequence in Figure 3 and the progression in Figure 6. We note that the factor $\upsilon_\beta + 1$ in eq 2 is responsible for the previously mentioned fact that the ground state transition is not the strongest in the progression. The resulting value for ν_β is included in Table I. Similarly, the result shown in Table I for ν_σ from microwave relative intensity measurements has been obtained from the $\upsilon_\sigma = 1$ satellite and the appropriate analogue of eq 2, that is from which the statistical weighting factor $\upsilon + 1$ is absent.

The $\upsilon_\beta = 1$ satellite in rotational transitions of HCN···HF is split into two components as a result of l-type doubling (see Figure 8). Nevertheless, its total intensity relative to the ground state is still given by eq 2 and leads to the value for ν_β recorded in Table I. The value of ν_σ determined by the above method is also included.[19]

Finally, further values of ν_β and ν_σ for HCN···HF are available, less directly, from interpretations of the l-type doubling constant q_β and the centrifugal distortion constant D_J, respectively. These interpretations are discussed in section IVE below but the results are included in Table I for convenience.

C. Rotational Constants and Vibration–Rotation Interaction Constants for ν_S, ν_σ, and ν_β

1. Ground-State Rotational and Centrifugal Distortion Constants from Microwave Spectroscopy

The ground-state rotational spectrum of HCN···HF has been measured for a large number of isotopic species[19,27] and hence provides a suitable example. The frequencies of transitions have been fitted by the familiar expression

$$\nu = 2B_0(J + 1) - 4D_J(J + 1)^3 \qquad (3)$$

to determine the rotational constants B_0 and the corresponding centrifugal distortion constants D_J shown in Table II. The two sets of constants with slightly lower accuracy were determined using Stark-modulation microwave spectroscopy[19] while the remainder were derived using the pulsed-nozzle, FT technique.[27]

2. Excited-State Spectroscopic Constants for ν_S, ν_σ, and ν_β

Rotational constants for the vibrationally excited states $\upsilon_\sigma = 1$ and $\upsilon_\beta = 1$ are readily determined[19] from

TABLE III. Excited State Spectroscopic Constants of HC^{14}N• • •HF

state	B_v, MHz	α_v, MHz	q, MHz
$v_S = 1$	3659.4 (10)	−68.3 (10)	–
$v_\sigma = 1$	3529.32 (2)	61.79 (3)	–
$v_\beta = 1$	3622.48 (9)	−31.25 (6)	12.9 (2)

the observed rotational spectra. Referring to the example of HC^{14}N···HF and the $J = 5 \leftarrow 4$ rotational transition shown in Figure 8, we note that the $v_\beta = 1$ satellite is split into two components of equal intensity and that satellites of higher v_β are also split into several components. The form of this $v_\beta = 1$ splitting is, in fact, characteristic of l-doubling, which results from the coupling of vibrational and rotational angular momenta in linear molecules. The frequencies of the two components of the $l = 1$ doublet are given by

$$\nu = 2B_v(J + 1) \pm \tfrac{1}{2}q_\beta(v_\beta + 1)(J + 1) - 4D_v(J + 1)\{(J + 1)^2 - l^2\} \quad (4)$$

where q_β is the l-doubling constant for the mode v_β and l is the quantum number associated with vibrational angular momentum along the molecular axis that results from the double degeneracy of v_β. For $|l| > 1$, the splitting is much smaller and much less readily described but the components are nevertheless conveniently labeled with the notation $(v_\sigma, v_\beta^{|l|})$ in Figure 8. By use of eq 4, B_v, D_v, and q_β for $v_\beta = 1$ have been evaluated[19] from observed rotational transition frequencies and are shown in Table III together with a value of α_β defined by the expression

$$B_v = B_0 - \alpha v \quad (5)$$

The determination of B_v for $v_\sigma = 1$ is similarly straightforward and its value is given in Table III along with α_σ.

The rotational spectrum of HCN···HF in the state $v_S = 1$ has not been observed because of an adverse Boltzmann factor but the rotational constant for this state, and hence a value of α_S, is available from the analysis of the rotational fine structure in the $v_\beta v_\beta + v_S \leftarrow v_\beta v_\beta$ band (see Figure 15a) by Bevan et al.[13a] The results are given in Table III. No such analysis is yet published for the $v_\beta v_\beta + v_B \leftarrow v_\beta v_\beta$ band and no satellites associated with v_B have been reported in the rotational spectrum. Hence spectroscopic constants for the mode v_B are not yet available and this is the situation for all hydrogen-bonded dimers so far investigated, but see section IID2.

D. Nuclear Hyperfine Coupling Constants for the Vibrational Ground State

The pulsed-nozzle, FT, and MBERS techniques enjoy sufficiently high resolution and sensitivity that various types of nuclear hyperfine structure can often be resolved in the rotational transitions of hydrogen-bonded dimers (see Figures 11–13, for such structure in rotational transitions of HCN···HF). For example, accurate values of nuclear quadrupole and nuclear spin–nuclear spin coupling constants have been determined by these methods.[27] Such coupling constants can be informative about the internal dynamics of the dimer and about electrical changes that accompany dimer formation. The interpretation of coupling constants in terms of these dimer properties is discussed in sections IVF and

IVG. We limit the discussion to dimers that are linear at equilibrium and concentrate our attention on HC-N···HF.

Nuclear quadrupole hyperfine structure arises from the coupling of the angular momentum I associated with a given nucleus to that J of the overall rotational motion. The mechanism of the coupling is the interaction of the nuclear electric quadrupole moment (nonzero if $I > 1/2$) with any electric field gradient that exists at the nucleus. For the special case of a linear dimer carrying a single quadrupolar nucleus, if the rotational spectrum in the hypothetical equilibrium state were available, the quantity obtained from the hyperfine structure would be the diagonal component χ_{zz} of the nucleus quadrupole coupling tensor, where z is the molecular axis. χ_{zz} is then simply related to the electric field gradient $q_{zz} = (\partial^2 V/\partial z^2)$ at the nucleus in question along z by

$$\chi_{zz} = -eQq_{zz}/h \quad (6)$$

where eQ is the nuclear electric quadrupole moment. Thus if χ_{zz} were available for, say, the nucleus at the binding center in the linear dimer before and after dimer formation, direct evidence about electric charge redistribution would result. Unfortunately, the observed quantity for a linear species is the diagonal component χ_{aa} in the zero-point state. There are difficulties in separating the contributions that electrical and zero point effects make to changes in χ_{aa} values observed when dimers are formed and these will be discussed below.

Nuclear spin–nuclear spin hyperfine structure results from the direct coupling of two nuclear spin angular momenta I_1 and I_2 by the interaction of their nuclear magnetic dipole moments. For a linear molecule in its hypothetical equilibrium state, the quantity derived from the spin–spin hyperfine structure in rotational transitions arising from the coupling of a pair of nuclei 1 and 2 would be the component D_{zz}^{12} of the coupling tensor, given by

$$D_{zz}^{12} = -2g_1g_2\mu_N^2/r^3 \quad (7)$$

where g_1 and g_2 are the nuclear g factors, μ_N is the nuclear magneton, and r is the equilibrium distance between nuclei 1 and 2. If we restrict consideration to the case of a diatomic molecule bound in a linear dimer, (e.g., HF in HCN···HF), the observed quantity for the free HF molecule can be written

$$D_0^{HF} = -2g_Hg_F\mu_N^2\langle 1/r^3\rangle_{0,0} \quad (8)$$

where the average is over the zero point motion. When the HF molecule is bound in the dimer, the observed quantity is the diagonal element D_{aa}^{HF} of the coupling tensor referred to the principal inertial axis system. In general, D_0^{12} and D_{aa}^{12} differ because of changes in $\langle 1/r^3\rangle$ on dimer formation and because zero point motion in the dimer takes the diatomic molecule away from the linear axis z. Again, the difficulty is to differentiate between the effect of bond length changes and zero point motion and this will be considered in section IV.

The hyperfine structures in the $J = 1 \leftarrow 0$ transitions of HC^{14}N···HF, HC^{15}N···HF, and HC^{15}N···DF shown in Figures 11, 12, and 13, respectively, have been analysed by methods discussed in detail elsewhere[27] to obtain the

TABLE IV. Nuclear Hyperfine Coupling Constants[a] for Various Isotopic Species of HCN• • •HF

coupling constant	HC^{14}N···HF	HC^{15}N···HF	HC^{15}N···DF	DC^{15}N···HF
$\chi_{aa}(^{14}$N), MHz	-4.098 (4)	-	-	-
$\chi_{aa}(D)$, kHz	-	-	269 (4)	186 (5)
D_{aa}^{HF}, kHz	-218 (6)	-242 (6)	-	-244 (4)

[a] Reference 27.

TABLE V. Stark Coefficients and Electric Dipole Moments for Various Vibrational States of H$_2$O• • •HF and D$_2$O• • •DF

vibrational state $(v_{\beta(o)}, v_{\beta(i)}, v_\sigma)$	rotational transition	$\Delta\nu/E^2$, 10^{-4} MHz V^{-2} cm^2	second-order Stark coefficient, 10^{-6} D^{-2} MHz V^{-2} cm^2	μ, D
H$_2$^{16}O···HF				
(0,0,0) ground state	$2_{11} \leftarrow 1_{10}$ $|M| = 0$	0.3575 ± 0.0023	2.1700	4.059 ± 0.013
	$2_{02} \leftarrow 1_{01}$ $|M| = 1$	0.3603 ± 0.0024	2.1787	4.067 ± 0.014
	$2_{12} \leftarrow 1_{11}$ $|M| = 0$	0.3648 ± 0.0023	2.1887	4.083 ± 0.013
(1,0,0)	$2_{02} \leftarrow 1_{01}$ $|M| = 0$	-0.3860 ± 0.0031	-2.6604	3.809 ± 0.016
	$2_{02} \leftarrow 1_{01}$ $|M| = 1$	0.3122 ± 0.0015	2.1616	3.796 ± 0.009
(0,1,0)	$2_{02} \leftarrow 1_{01}$ $|M| = 1$	0.3608 ± 0.0029	2.1737	4.074 ± 0.016
D$_2$^{16}O···DF				
(0,0,0) ground state	$2_{02} \leftarrow 1_{01}$ $|M| = 0$	-0.466 ± 0.011	-2.9497	3.97 ± 0.05

nuclear hyperfine coupling constants $\chi_{aa}(^{14}$N), D_{aa}^{HF}, and $\chi_{aa}(D)$ listed in Table IV. (Nuclear spin–nuclear spin coupling involving the other $I = {}^1/_2$ particles is too small to detect.)

E. Stark Coefficients from the Splitting of Rotational Transitions in Applied Electric Fields

It is well known[31] that the rotational transitions of linear molecules and asymmetric rotor molecules generally exhibit a second-order Stark effect, that is the rotational energy levels are displaced from their zero-field values by an energy proportional to μ^2E^2, where μ is the appropriate molecular electric dipole moment and E is the strength of the applied static, uniform electric field. As a result, the so-called Stark components into which a rotational transition correspondingly splits are displaced $\Delta\nu$ in frequency from the zero field value such that $\Delta\nu$ is proportional to μ^2E^2. As an example, we show in Figure 16 how the frequency displacement $\Delta\nu$ varies with E^2 for some Stark components of the hydrogen-bonded dimer H$_2$O···HF in various vibrationally excited states and for D$_2$O···DF in its ground state.[32] In Figure 16, the notation $(v_{\beta(o)}, v_{\beta(i)}, v_\sigma)$ is used to label the vibrational state in question (see section IIA1 for a discussion of nomenclature). The heterodimer H$_2$O···HF is an effectively planar asymmetric rotor[20,33,34] and the observed straight lines confirm the behaviour alluded to above. The slope of each straight line $\Delta\nu/E^2$ is called the Stark coefficient of the component in question and allows μ, the electric dipole moment, of the dimer to be determined (see section IVD). A selection of Stark coefficients for H$_2$O···HF and D$_2$O···DF is given in Table V.

The measurements referred to in Table V and Figure 16 were made on an equilibrium gas mixture of H$_2$O and HF using a Stark-modulation microwave spectrometer configured to allow the selection rule $\Delta M = 0$. In fact, even more accurate measurements of Stark coefficients, and hence electric dipole moments, result from MBERS. For example, Klemperer et al.[22] have determined the value $\mu_a = 2.98865$ (9) D for the HF dimer.

Quadratic Stark effects, such as those shown above, are expected for a linear molecule and are almost invariably observed. Indeed, the $M = 3$ component of the $J = 4 \leftarrow 3$ transition of HC^{14}N···HF behaves in this manner.[35] On the other hand, it was found[36] for several
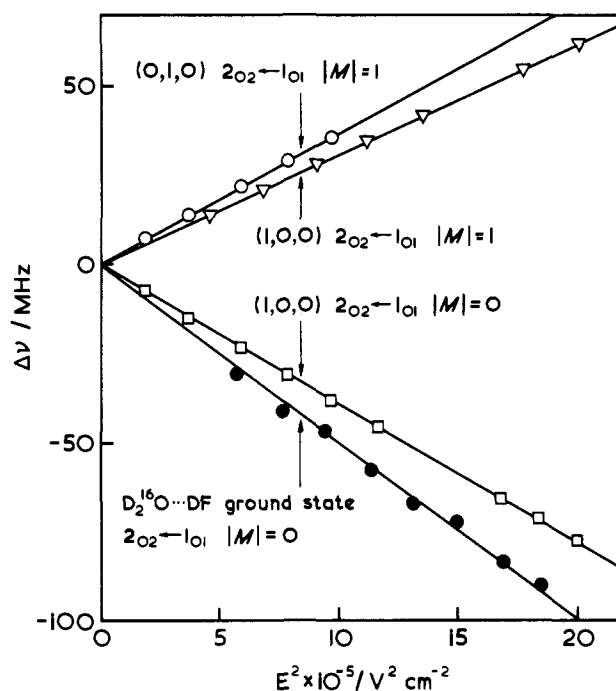
Figure 16. Observed second-order frequency shifts $\Delta\nu$ as a function of the square of the electric field strength E^2 for H$_2$O···HF and D$_2$O···DF. See the text for the labeling scheme of vibrational states. Redrawn with permission from ref 32. Copyright 1983 American Institute of Physics.
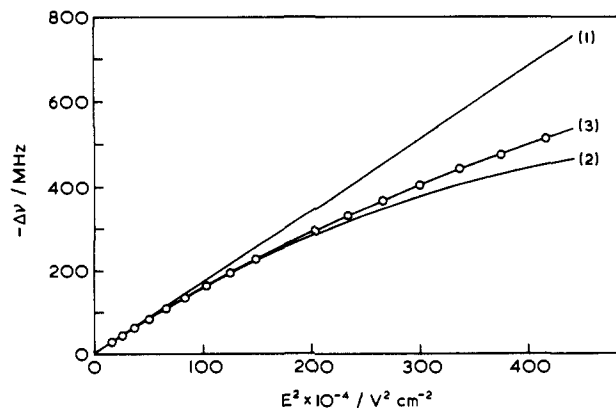
Figure 17. Stark effect for the transition $M_J = 0$, $J = 2 \leftarrow 1$ of HCN···HF. Calculated (1) by second-order perturbation theory, (2) by second- and fourth-order perturbation theory, (3) by matrix diagonalization. The points O represent experimental observations. Redrawn with permission from ref 36. Copyright 1978 Academic Press.

TABLE VI. Electric Dipole Moment of $HC^{14}N \cdot \cdot \cdot HF$

$J + 1 \leftarrow J$	M		μ, D
$2 \leftarrow 1$	0		5.627
	1		5.601
$4 \leftarrow 3$	3		5.608
		mean	5.612

other transitions that a plot of $\Delta\nu$ vs. E^2 exhibits a pronounced curvature. This is clearly seen for the $M = 0$ component of the $J = 2 \leftarrow 1$ transition in Figure 17 when $\Delta\nu$ is plotted against E^2. A quadratic Stark effect for a linear molecule is predicted on the basis of second order perturbation theory with the neglect of higher order terms. However, higher order terms are negligible only when the rotational constant of the molecule is sufficiently large and the electric dipole moment is relatively small. This is not so for HCN···HF for which $\mu = 5.612$ D and $B_0 = 3.573$ GHz. In this case, a complete diagonalization of the Hamiltonian matrix for the linear rotor in the applied electric field is necessary rather than a perturbation treatment truncated at second order.[36] The result of the complete analysis is consistent with the observed Stark effect for the $M = 0$ component of the $J = 2 \leftarrow 1$ transition (see Figure 17) and when applied to other transitions results in internally consistent values of the electric dipole moment, as shown in Table VI.

F. Number Densities of HCN, HF, and HCN···HF In Equilibrium Mixtures from Absolute Intensity Measurements

The measurement of the absolute (or integrated) intensity of a rotational transition in each of HCN and HCN···HF in an equilibrium mixture of HCN,HF, and HCN···HF allows a determination of the number density $n_{0,0}$ in the rotational and vibrational ground state for each species present.[19,37] As we shall discuss in section IVF, this provides a route to the equilibrium dissociation energy D_e of HCN···HF.

For a transition originating in a state characterized by vibrational and rotational quantum number v and J, respectively, the absolute (or integrated) line intensity is given by

$$I = (8\pi^3 n_{v,J}/3ckT)|\mu_{ij}|^2\nu_0^2 \qquad (9)$$

where $n_{v,J}$ is the number of molecules per unit volume in the state v,J, and ν_0 is the frequency of the transition. Thus, if μ is known, $n_{v,J}$ can be determined directly and uniquely from absolute intensity measurements of rotational transitions in high resolution spectra because expressions for $|\mu_{ij}|^2$ in terms of μ are available. For example, in the case of the $J + 1 \leftarrow J$ transition of a linear molecule in its ground vibrational state

$$|\mu_{ij}|^2 = \mu^2(J + 1)/(2J + 1) \qquad (10)$$

Since the rotational constant and the vibrational frequencies are experimentally known for each of B = HCN, HF, and HCN···HF, it is possible to use the well-known expressions for the various partition functions to calculate the $n_{0,0}(B)$ from the $n_{v,J}(B)$. Given the $n_{0,0}(B)$ values, the quantity $K_{0,0}$ defined as

$$K_{0,0} = n_{0,0}(HCN\cdots HF)/n_{0,0}(HCN)n_{0,0}(HF) \qquad (11)$$
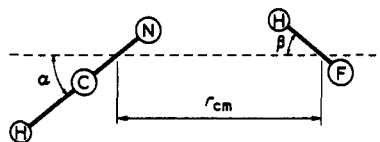
can be calculated. As we shall indicate later, $K_{0,0}$ is

Figure 18. Model used in discussion of the zero-point motion of HCN···HF.

simply related to the zero-point dissociation energy D_0 of HCN···HF. Absolute intensity measurements were used to determine the partial pressure of HCN and HCN···HF in the mixture, from which the partial pressure of HF follows by difference from the total pressure. The partial pressure and hence the number density $n(HCN)$ of HCN in a given mixture of HCN and HF was determined from the measured area of the $J = 12$, $v_2 = 1$, l doublet transition at 34 953.8 MHz by using a calibration curve constructed for the same transition in pure hydrogen cyanide. The partial pressure of the dimer was obtained from the absolute intensity of the $J = 4 \leftarrow 3$ transition in the vibrational ground state.

IV. Determination of Molecular Properties from Spectroscopic Quantities

A. The Zero-Point Oscillation of the Subunits in HCN···HF from Nuclear Hyperfine Coupling Constants

Many of the spectroscopic quantities discussed in section III refer to the zero-point states of hydrogen-bonded dimers. Moreover, the vast majority of the information presented in section III pertains to the linear species HCN···HF and accordingly the discussion in this Section will be concerned mainly with the determination of the molecular properties of HCN···HF from zero-point quantities. Because of the relatively weak intermolecular interaction, the zero-point amplitudes of the subunits are larger than is normally the case and consequently it is desirable both to estimate their magnitude and to allow for them when interpreting spectroscopic quantities. The observed nuclear hyperfine coupling constants provide a route to estimating the amplitude of the angular oscillation of each subunit in HCN···HF with respect to its mass center. We must therefore discuss next a model of the zero-point motion which allows this interpretation and then examine the molecular properties that follow from other spectroscopic constants in the light of this model.

We shall use a model of the type shown in Figure 18, that is linear at equilibrium but with the HCN and HF subunits undergoing relatively large amplitude oscillatory motions in the zero-point state about their respective centers of mass.[27] The subunits are assumed to be rigid. The motions are then defined by the angular displacements α and β and, because of the cylindrical symmetry, each nucleus describes a circle in the plane perpendicular to the molecular axis. We also assume that r_{cm}, the distance between the subunit mass centers, does not change significantly during the zero-point motion.

If the electrical properties of one subunit were unaffected by the presence of the other subunit and the value of $r(H-F)$ was not significantly changed on dimer formation, an observed nuclear hyperfine coupling

TABLE VII. Molecular Geometry of HCN• • •HF

isotopic species	$\langle r_{cm}{}^2 \rangle^{1/2}$, Å	$r(N \cdots F)$, Å[a]
$HC^{15}N \cdots HF$	3.3260	2.8049
$HC^{14}N \cdots HF$	3.3462	2.8043
$DC^{15}N \cdots HF$	3.3820	2.8048
$HC^{15}N \cdots DF$	3.2811	2.8017
$HC^{14}N \cdots DF$	3.3014	2.8011
$DC^{14}N \cdots DF$	3.3371	2.8015

[a] $r(N \cdots F) = \langle r_{cm}{}^2 \rangle^{1/2} + r \cos \beta - r' \cos \alpha$. See text for discussion.

constant C_{aa} would be related to C_0 that of the free subunit by

$$C_{aa} = \tfrac{1}{2}C_0 \langle 3 \cos^2 \tau - 1 \rangle \qquad (12)$$

where τ is the angle between the instantaneous a-axis of the dimer and the symmetry axis of the appropriate subunit. The angles τ are defined in Figure 18, that is α for HCN and β for HF. (This assumes that the a-axis and the line between the mass centers coincide. They do not but the angle between them is negligibly small for present purposes). From eq 12 $\langle \cos^2 \alpha \rangle$ can be evaluated from the coupling constant $\chi_{aa}(D)$ in $DC^{15}N \cdots HF$, which has been included for convenience in Table IV, and $\langle \cos^2 \beta \rangle$ from $D_{aa}{}^{HF}$. This interpretation has to be qualified in two respects. While the electric field gradient at D in $DC^{15}N \cdots HF$ is formally perturbed by the presence of the HF subunit, corrections for this effect are negligible in this case because of the remoteness of the D-nucleus. On the other hand, the value of $D_{aa}{}^{HF}$, and hence $\langle \cos^2 \beta \rangle$, must be corrected for a small (0.014 Å) lengthening of the HF bond on formation of the dimer (see section IVC). The corrected values are $\langle \cos^2 \alpha \rangle = 0.9710$ and $\langle \cos^2 \beta \rangle = 0.9423$. This provides the basis of the model of the zero-point motion in HCN$\cdots$HF which is used in the next Section to discuss the determination of $r(N \cdots F)$. This value of $r(N \cdots F)$ is, of course, influenced by zero-point averaging over the contribution of the remaining dimer modes, particularly ν_σ, the stretching of the hydrogen bond.

B. The r_0-Geometry of HCN$\cdots$HF from Rotational Constants

It has been established beyond doubt from the magnitude of the rotational constants B_0 for a large number of isotopic species of HCN$\cdots$HF (see Table II) that the nuclei lie in the order indicated.[19] The nature of the vibrational satellite pattern in the ν_β progression for each rotational transition (see Figure 8), and in particular the presence of the characteristic l doubling, establishes that the equilibrium geometry is linear. In the approximation defined by the model discussed in section IVA, the ground state moments of inertia I_b, $I_b{}^{HCN}$ and $I_b{}^{HF}$ of the dimer, free HCN and free HF, respectively, are related by[27]

$$I_b \approx \langle I \rangle = \mu \langle r_{cm}{}^2 \rangle + \tfrac{1}{2}I_b{}^{HCN}(1 + \langle \cos^2 \alpha \rangle) + \tfrac{1}{2}I_b{}^{HF}(1 + \langle \cos^2 \beta \rangle) \qquad (13)$$

where $\mu = m_{HCN}m_{HF}/(m_{HCN}+m_{HF})$ and angular brackets denote the zero-point average. The values of $\langle r_{cm}{}^2 \rangle^{1/2}$ obtained by using the rotational constants from Table II in eq 13 are given for each isotopic species investigated in Table VII. The distance $r(N \cdots F)$ between the planes of the circles described by the N and F nuclei can then be determined for each isotopic species from

the expression $r(N \cdots F) = \langle r_{cm}{}^2 \rangle^{1/2} + r \cos \beta - r' \cos \alpha$, where r' and r are the distances of N from the center of mass of HCN and F from the center of mass of HF, respectively. The values of $r(N \cdots F)$, but not $\langle r_{cm}{}^2 \rangle^{1/2}$, have a high internal consistency over a range of isotopic species.

C. Lengthening of the H–F Bond on Formation of HCN$\cdots$HF from Nuclear Hyperfine Coupling Constants

It is possible by using the dynamical model discussed in section IVA, the known electric charge distributions of HCN and HF, and the nuclear hyperfine coupling constants given in section IIID to determine the lengthening δr of the HF bond that accompanies incorporation of HF into HCN$\cdots$HF.[27]

In order to discuss the determination of δr, we begin[38,39] by defining the "effective" coupling constants of a free H(D)F molecule stretched by δr, that is $\chi_0{}^{eff}$ for the D-nuclear quadrupole coupling constant and $D_0{}^{eff}$ for the H,F nuclear spin–nuclear spin coupling constant. We denote the proper free molecule values as χ_0 and D_0, respectively. With these definitions, it then follows that the observed H,F spin–spin coupling constant $D_{aa}{}^{HF}$ in HCN$\cdots$HF is related to $D_0{}^{eff}$ by the familiar equation

$$D_{aa}{}^{HF} = \tfrac{1}{2}D_0{}^{eff}\langle 3 \cos^2 \beta^H - 1 \rangle \qquad (14)$$

where β^H is the angle between the instantaneous a-axis of the dimer and the HF internuclear line and the average is over the zero-point motion. The quantities D_0 and $D_0{}^{eff}$ introduced above are related by

$$D_0{}^{eff} = D_0 + \frac{dD_0}{dr} \cdot \delta r \qquad (15)$$

if δr is sufficiently small. The derivative $dD_0/dr = 9.2$ kHz/0.01 Å follows directly from the geometry of HF because D_0 is defined in terms of r by eq 8. Relationship 14 is exact because $D_{aa}{}^{HF}$ is unaffected by electrical effects due to HCN.

On the other hand, for the D-nuclear quadrupole coupling constant, the analogous equation must be written

$$\chi_{aa}{}^{corr} = \tfrac{1}{2}\chi_0{}^{eff}\langle 3 \cos^2 \beta^D - 1 \rangle \qquad (16)$$

where $\chi_{aa}{}^{corr}$ is the D-nuclear quadrupole coupling constant in the dimer but corrected for the contribution of B to the electric field gradient at D. For the HCN$\cdots$DF dimer discussed below, $\chi_{aa}{}^{corr}$ differs by a small but (in some cases) significant amount from the observed value χ_{aa}. The method of calculating $\chi_{aa}{}^{corr}$ from χ_{aa} using a distributed point multipole model to represent the electric charge distribution of B is discussed elsewhere.[39] By analogy with eq 15, we write

$$\chi_0{}^{eff} = \chi_0 + \frac{d\chi}{dr} \cdot \delta r \qquad (17)$$

where $d\chi/dr$ is available by scaling[40] the results of an ab initio calculation[41] and has the value -33 kHz/0.01 Å. From eq 14–17, if the relationship between β^H and β^D is known, it is possible to determine a value for δr.

The relationship between β^H and β^D is provided by a two-dimensional isotropic, harmonic oscillator de-
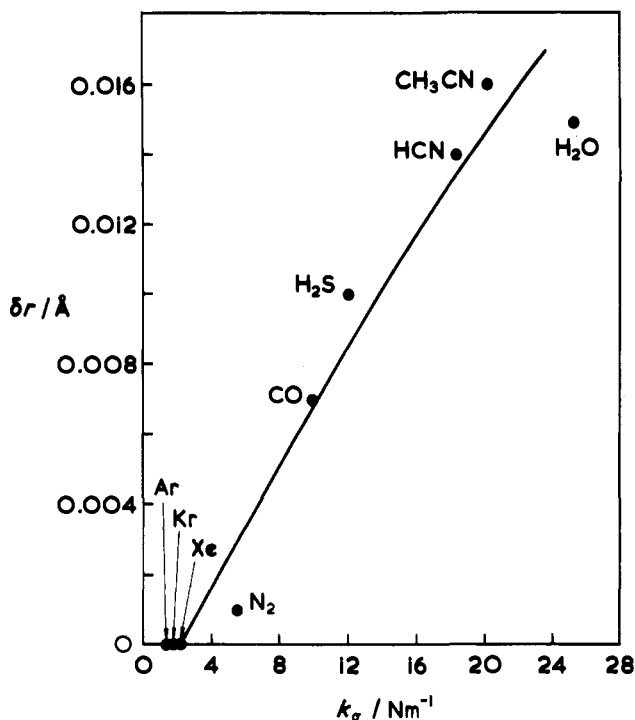
Figure 19. The variation of δr with the intermolecular stretching force constant k_σ along the series B···HF, where B = Ar, Kr, Xe, N_2, CO, H_2S, HCN, CH_3CN, and H_2O. Redrawn with permission from ref 39. Copyright 1986 Royal Society (London).

scription of the motion of the H(D)F subunit. This model leads to the relationship

$$\beta_{av}^D \approx \beta_{av}^H (\mu_{HF}/\mu_{DF})^{1/4} \tag{18}$$

where β_{av} is defined operationally according to

$$\beta_{av} = \cos^{-1} \langle \cos^2 \beta \rangle^{1/2} \tag{19}$$

Application of the model to the system ArHF/ArDF shows that $\chi_0^{eff} = \chi_0$, $D_0^{eff} = D_0$ and $\chi_{aa}^{corr} = \chi_{aa}$ to a sufficient approximation, as expected if the model is satisfactory. The lengthening δr for HCN···HF is calculated[27] on the above basis to be 0.014 Å. The calculation is readily extended[39] to a variety of dimers B···HF where B = Ar, Kr, Xe, N_2, CO, H_2S, HCN, CH_3CN, and H_2O. The values of δr are zero for the first three members of the series and then 0.001, 0.007, 0.010, 0.014, 0.016, and 0.015 Å, respectively. It is revealing to plot δr against the intermolecular stretching force constant k_σ as a convenient measure of the strength of the hydrogen bond (the method of determination of k_σ is given in section IVE). This plot is shown in Figure 19 from which it is immediately clear that δr is a smoothly increasing function of k_σ and hence of the intermolecular binding strength.

D. Electrical Changes Accompanying Dimer Formation from Electric Dipole Moments and Nuclear Quadrupole Coupling Constants

Electric charge rearrangement that accompanies formation of a dimer B···HA is an important characteristic of the hydrogen bond. Some information about the electric charge rearrangement is available from two properties discussed in earlier sections, namely the electric dipole moment of the dimer in comparison with those of the separate components and the nuclear

TABLE VIII. Electric Dipole Moment Components and the Enhancements, $\Delta\mu_a$, of Hydrogen-Bonded Dimers

dimer	μ_a, Debye	$\Delta\mu_a$, Debye	ref
HF···HF	2.98865 (9)	0.60	22
H_2O···H_2O	2.6429 (2)	0.46	21
H_2O···HF	4.073 (7)	0.68	32
HF···HCl	2.4095 (5)	0.14	42
H_2S···HF	2.6239 (17)	0.78	43
HCN···HF	5.612 (10)	0.80	36
$(CH_2)_2O$···HF	3.85 (2)	0.99	44
N_2O···HF	2.069 (4)	–	45
CO_2···HF	2.2465 (4)	0.60	46
SCO···HF	3.208 (2)	0.84	46

quadrupole coupling constants in certain specially chosen dimers.

1. The Enhancement of the Electric Dipole Moment on Dimer Formation

The electric dipole moments of dimers such as HCN···HF and H_2O···HF have been determined from measurements of the Stark effect[32,35,36] (see section IIIE). These can be interpreted on the basis of models for the internal dynamics of the subunits of the type discussed in section IVA to give the enhancement of the electric dipole moment over the vector sum of the component dipole moments. We illustrate the procedure with HCN···HF before giving a table of such enhancements.

Given the model for the zero-point oscillation of the subunits in HCN···HF shown in Figure 18, it is clear that the electric dipole moment of the dimer can be written

$$\mu_{dimer} = \Delta\mu + \mu_{HCN}\langle\cos \alpha\rangle + \mu_{HF}\langle\cos \beta\rangle \tag{20}$$

where μ_{HCN} and μ_{HF} are the zero-point moments of the monomers and $\Delta\mu$ defines the enhancement of the electric dipole moment. For molecules of lower symmetry, straightforward modifications of this equation can be made. If we assume that $\langle\cos^2 \alpha\rangle \approx \langle\cos \alpha\rangle^2$ and $\langle\cos^2 \beta\rangle \approx \langle\cos \beta\rangle^2$, the corrected mean square values[27] given in section IVA and the appropriate μ_{HCN} and μ_{HF} values lead to $\Delta\mu = 0.897$ (10) D for HCN···HF. We show in Table VIII the enhancement of μ, or the a-component μ_a, as appropriate, for several dimers measured mainly by the MBERS technique.[42-46] These enhancements have contributions from the polarization of one subunit by the other and from any charge transfer on formation of the dimer.

2. Charge Redistribution within a Subunit from Nuclear Quadrupole Coupling Constants

The enhancement $\Delta\mu$ for HCN···HF contains information about charge redistribution in the HCN subunit brought about by the presence of the HF molecule. This charge redistribution will also be reflected in the magnitude of the ^{14}N-nuclear quadrupole coupling constant in the dimer but its contribution cannot be readily deconvoluted in the present state of knowledge. If, however, we consider the closely related linear dimer N≡N···HF we can draw conclusions[47] about the electrical changes on dimer formation from the two ^{14}N-nuclear quadrupole coupling constants because in this special case the two nitrogen nuclei are equivalent in the free component.

Accurate values $\chi_{aa}(1) = -4.978$ (3) MHz and $\chi_{aa}(2) = -4.697$ (2) MHz have been determined[47] for the two

^{14}N-nuclear quadrupole coupling constants in N(1)≡N(2)···HF by pulsed-nozzle, FT microwave spectroscopy. These are significantly different in the dimer, but necessarily equal in free nitrogen, and have been determined from a detailed analysis of the rotational spectra of ^{14}N^{15}N···HF and ^{15}N^{14}N···HF, respectively. Clearly, whatever zero-point excursions the nitrogen molecule undergoes on the basis of a model similar to that discussed above for HCN···HF, each observed value of $\chi_{aa}(n)$ results from the identical projection of its vibrationless counterpart on the a-axis. Consequently, the difference $\Delta\chi_{aa} = \chi_{aa}(1) - \chi_{aa}(2)$ is the lower limit to the equilibrium value of this quantity. In the following argument $\Delta\chi_{aa}$ is treated as if it were the equilibrium value.

Using an analysis which has been described elsewhere,[47,48] the known geometry of N_2···HF, the known electric multipole moment expansion of HF, and an estimated value of the Sternheimer shielding constant $(1 - \gamma_\infty)$ for the ^{14}N-nuclei have been used to evaluate the contribution $\Delta\chi_{aa}{}^{HF}$ to $\Delta\chi_{aa}$ that arises from the presence of the HF electric charge distribution. If the charge transfer from N_2 to HF is negligible, as in the rare gas analogues,[49] the corrected value $\Delta\chi_{aa}{}^P = \Delta\chi_{aa} - \Delta\chi_{aa}{}^{HF} = -0.33$ MHz can be assumed to result entirely from polarization of charge from N(1) to N(2) when HF achieves its equilibrium position in the dimer.

The value of $\Delta\chi_{aa}{}^P$ can be interpreted in terms of fractional electronic charge transfer from N(1) to N(2) on the basis of a simple valence bond model for molecular nitrogen. The values of the ^{14}N-nuclear quadrupole coupling constants have been estimated for each of the three valence bond structures of nitrogen N(1)≡N(2), N$^+$(1)=N̄(2), and N̄(1)=N$^+$(2) by using the Townes–Dailey method[31] to give $\Delta\chi$ values of 0, -12.5, and 12.5 MHz, respectively. On this basis, the observed value of -0.33 MHz corresponds to the transfer of 0.026 e from N(1) to N(2) as the dimer is formed. A similar treatment has been applied to C_2N_2···HF,[48] N_2···HCN,[50] and to N_2···HCl[51] and leads to estimated values of 0.025 e, 0.016 e, and 0.036 e, respectively.

E. Hydrogen-Bond Stretching and Bending Force Constants from Vibrational Spacings and from Vibration–Rotation Interaction Constants

1. Hydrogen-Bond Stretching Force Constants

There are two routes that have been used to determine the hydrogen bond stretching force constant k_σ from spectroscopically observed quantities. Both of these routes assume a pseudodiatomic model for the force field. The first involves the use of the vibrational separation $\nu_\sigma = 1 \leftarrow 0$ and the assumption of a harmonic oscillator model in which $\bar{\nu}_\sigma = (2\pi c)^{-1}(k_\sigma/\mu)^{1/2}$. The second makes use of the centrifugal distortion constant D_J, in the case of a linear or symmetric rotor dimer, or Δ_J for a planar asymmetric rotor. It has been shown, for example, that for a weakly bound dimer B···HA, having a linear equilibrium geometry and formed from a pair of rigid linear molecules, the centrifugal distortion constant D_J and the quadratic force constant k_σ are related by

$$D_J = \frac{16\pi^2 B_0{}^3}{k_\sigma}\mu\left(1 - \frac{B_0}{B_B} - \frac{B_0}{B_{HA}}\right) \quad (21)$$

TABLE IX. Hydrogen Bond Stretching Force Constants k_σ for Dimers B • • •HF

dimer	D_J or Δ_J, kHz	k_σ, Nm^{-1}	ref
Ar···HF	70.90 (6)	1.41	53
OCO···HF	10.69 (7)	2.2	46
^{15}N$_2$···HF	16.0	5.51	47
OC···HF	9.77	8.96	54
H$_2$S···HF	15.10 (22)	12.04	55
HC^{15}N···HF	6.97 (2)	18.26	27
CH$_3$C^{15}N···HF	0.90 (1)	20.1	56
H$_2$O···HF	35.5 (9)	25.3	34

TABLE X. Angle-Bending Force Constants (10^{-20} J rad^{-2}) for the Methyl Cyanide-Hydrogen Fluoride Dimer

	^{12}CH$_3$^{12}C^{14}N···H^{19}F		
$k_{\theta\phi}$	$k_{\theta\theta}$	$k_{\phi\phi}$	D_{JK}
-2.0	3.4	6.6	59.0
-1.0	2.6	7.5	63.8
0.0	2.3	8.3	68.5
1.0	2.2	9.0	73.1
2.0	2.4	9.6	77.6

R—C≡N···H—F
ω θ φ

Figure 20. Labeling of internal coordinates of CH$_3$CN···HF.

where B_0, B_B, and B_{HA} are the ground-state rotational constants of the dimer, of B and of HA, respectively. This model has been generalized[52] to include dimers that are planar asymmetric rotors of C_{2v} symmetry when Δ_J is the appropriate centrifugal distortion constant.

For HCN···HF, the $\nu_\sigma = 1 \leftarrow 0$ vibrational spacing of 155 (10) cm^{-1} from the infrared spectrum[10] (see Table I) leads to $k_\sigma = 16.3$ (5) Nm^{-1} while the centrifugal distortion constant for HC^{15}N···HF (see Table II) gives 18.26 (5) Nm^{-1} when appropriately employed in eq 21.[27] We show in Table IX k_σ values determined for a selection of hydrogen-bonded dimers B···HF by use of eq 21 or its analogue.

2. Hydrogen-Bond Bending Force Constants

The most complete determination of the quadratic bending force constants for a hydrogen-bonded dimer has been made[18] in the case of CH$_3$CN···HF. In this analysis, the methyl group was treated as a point mass and the internal coordinates θ, ϕ, and ω, as defined in Figure 20, were used to describe the three bending modes, namely the RCN bend and the two hydrogen-bond bending modes ν_B and ν_β. The GF matrix method was applied to this five-atom model and, after setting all off-diagonal elements of the F-matrix other than $k_{\theta\phi}$ to zero, the values of $k_{\theta\theta}$, $k_{\phi\phi}$ and $k_{\omega\omega}$ which reproduce the observed bending wavenumbers were determined for a range of assumed $k_{\theta\phi}$ values. The observed bending wavenumbers used were $\bar{\nu}_\beta = 42.5$ cm^{-1}, $\bar{\nu}_B = 620$ cm^{-1} and $\bar{\nu}_\omega = 361$ cm^{-1} (the last assumed unchanged from free CH$_3$CN). The results of this procedure are given in Table X. Any row within Table X satisfies the observed bending wavenumbers but a unique solution is defined if we apply the additional constraint that the bending force field must reproduce the centrifugal distortion constant $D_{JK} = 67$ (2) kHz for CH$_3$CN···HF which has been determined from the rotational spectrum using eq 1 (see section IIB2). The means of calculating D_{JK} from the force field is discussed elsewhere.[57] As a result of this procedure, it is found[18] that
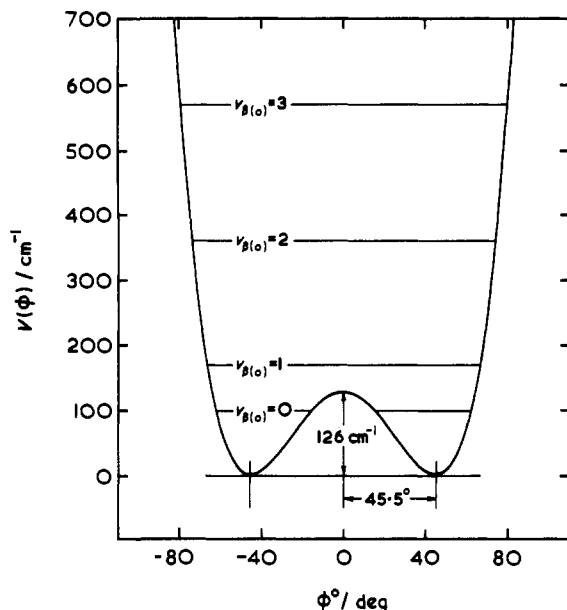
Figure 21. The potential energy function governing the mode $\nu_{\beta(o)}$ in $H_2O\cdots HF$. Redrawn with permission from ref 20. Copyright 1982 Royal Society (London).

$k_{\theta\phi}$ is zero within experimental error and hence that $k_{\theta\theta}$ = 2.4 (2) $\times$ 10^{-20} J rad^{-2} and $k_{\phi\phi}$ = 8.0 (7) $\times$ 10^{-20} J rad^{-2}. If we make the assumption that the cross term $k_{\theta\phi}$ is also zero in $HCN\cdots HF$ (where the constraint imposed by D_{JK} is not available), a similar analysis leads[19] to $k_{\theta\theta}$ = 3.7 $\times$ 10^{-20} J rad^{-2} and $k_{\phi\phi}$ = 6.3 $\times$ 10^{-20} J rad^{-2}. The only other case[58] where such force constants have been obtained is for the in-plane bending modes $\nu_{\beta(i)}$ and $\nu_{B(i)}$ of $H_2O\cdots HF$. For this dimer, $k_{\theta\theta}$ = 2.52 $\times$ 10^{-20} J rad^{-2} and $k_{\phi\phi}$ = 9.85 $\times$ 10^{-20} J rad^{-2}. Thus, in all three dimers, it is found that bending at the hydrogen atom is more strongly resisted than bending at the heavy atom.

The lower symmetry of the hydrogen-bonded hetero-dimer $H_2O\cdots HF$ by comparison with $HCN\cdots HF$ and $CH_3CN\cdots HF$ leads to a distinction between the in-plane bending modes [$\nu_{\beta(i)}$ and $\nu_{B(i)}$] and the out-of-plane bending modes [$\nu_{\beta(o)}$ and $\nu_{B(o)}$]. In fact, the out-of-plane, low frequency mode $\nu_{\beta(o)}$ is highly anharmonic as indicated by the vibrational separations 64 $\pm$ 10 cm^{-1} for $\nu_{\beta(o)}$ = 1 $\leftarrow$ 0 and 203 (35) cm^{-1} for $\nu_{\beta(o)}$ = 2 $\leftarrow$ 1 obtained[20] from relative intensity measurements of the appropriate vibrational satellites in the rotational spectrum of $H_2O\cdots HF$. A strongly anharmonic potential energy function governing the mode $\nu_{\beta(o)}$ is thus indicated and is confirmed by the behavior both of the rotational constants and the electric dipole moment (see Table V) with successive excitation of $\nu_{\beta(o)}$. In the one-dimensional approximation, it has been possible to determine[20] a potential energy function of the type $V(\phi)$ = $\alpha\phi^4 + \beta\phi^2$ by fitting the observed vibrational spacings, rotational constants, and electric dipole moments. The angle ϕ is defined as the angle between the O$\cdots$F line and the bisector of the HOH angle in $H_2O\cdots HF$. The form of $V(\phi)$ is shown in Figure 21. This establishes that the equilibrium value of ϕ is 45.5° and that the equilibrium geometry of $H_2O\cdots HF$ has C_s symmetry. In the zero-point state, on the other hand, the molecule is effectively planar, since the vibrational wave function has C_{2v} symmetry.

The conclusion for $H_2O\cdots HF$ can be rationalized on the basis that at equilibrium the HF molecule lies along

$n_{0,0}(HCN)$	7.86 $\times$ 10^{18} m^{-3}
$n_{0,0}(HF)$	4.15 $\times$ 10^{20} m^{-3}
$n_{0,0}(HCN\cdots HF)$	2.14 $\times$ 10^{13} m^{-3}
$K_{0,0}$	0.656 $\times$ 10^{-26} m^{-3}
D_0	18.6 kJ mol^{-1}

the axis of a nonbonded electron pair on oxygen, as conventionally envisaged (see section V). The hetero-dimers oxirane$\cdots$HF and oxetane$\cdots$HF are also of interest in this respect. The ground-state rotational constants lead to the values for the angle ϕ (defined as for $H_2O\cdots HF$) of 72° and 52° for the oxirane[44] and ox-etane[59] complexes, respectively. The nonbonded pair interpretation readily rationalizes the increase in angle ϕ as the CÔC angle decreases from oxetane to oxirane.

As mentioned earlier (section IIIB2) the l-doubling constant q_β for $HCN\cdots HF$ offers another method of obtaining ν_β. The constant q_β is related, in the harmonic approximation, to the vibrational frequencies ν_i of the molecule and the Coriolis coupling constants $\zeta_{\beta i}$ by

$$q_\beta = \frac{2B_e^2}{\nu_\beta}[1 + 4\Sigma_i \zeta_{\beta i}^2 \nu_i^2/(\nu_i^2 - \nu_\beta^2)] \qquad (22)$$

Evaluation of the $\zeta_{\beta i}$ through the usual matrix methods and use of these with the known vibrational frequencies of $HCN\cdots HF$ and q_β in eq 22 leads[60] to a value $\bar{\nu}_\beta$ = 72 cm^{-1} which can be compared with those available by other methods in Table I.

Finally, a further source of information about the bending motion is available from the oscillation amplitudes α_{av} and β_{av} of the subunits. Values of such amplitudes have been obtained for numerous dimers from measurements of hyperfine coupling constants χ and D, by using the operationally defined angles as in eq 19. It is now clear that account has to be taken of H–A bond lengthening in the use of nuclear spin–nuclear spin interaction constants and also of the effect of the electric charge distribution of B on H–A in the use of nuclear quadrupole coupling constants. When such allowances can be made it becomes possible[61] to use the oscillation amplitudes to assist in the evaluation of bending force constants of the dimer.

F. Hydrogen-Bond Dissociation Energies from Absolute Intensities of Rotational Transitions

As discussed in section IIIF, the measurement of the absolute intensity of a rotational transition of two of the components B,HA and B$\cdots$HA in a gaseous equilibrium mixture of the components provides a method of determining the number density $n_{0,0}$ in the rotational and vibrational ground state for each of the species present. It is then readily shown[19,37] that the zero-point equilibrium constant $K_{0,0}$, defined in terms of $n_{0,0}$ according to eq 11 and measured as discussed in section IIIF, is related to the zero-point dissociation energy D_0 for the reaction

$$B\cdots HA = B + HA \qquad (23)$$

by

$$K_{0,0} = n_{0,0}(B\cdots HA)/n_{0,0}(B)n_{0,0}(HA) =$$
$$(h^2/2\pi\mu kT)^{3/2}\exp(D_0/RT) \qquad (24)$$

TABLE XII. Summary of Hydrogen-Bonded Dimers B • • • HA Investigated by Rotational and Vibrational Spectroscopy
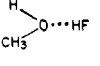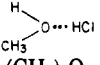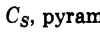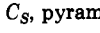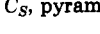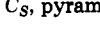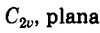
| proton acceptor, B	proton donor, HA	equilibrium geometry	ref {type of spectrum: derived properties}[a]
A		A. Nonbonded Pair as Acceptor; Linear and Symmetric Top Species	
HCN	HF	linear, $C_{\infty v}$, HCN···HF	10 {IR: ν_S, ν_B, ν_σ, ν_β}; 19 {mw: B_0, B_v, CD, ν_β, ν_σ, μ, D_e, r(N···F)}; 27 {B_0, CD, χ(^{14}N), χ(D); D^{HF}, r(N–F)}; 13 {IR: ν_S, B_v, r'(N···F)}
	HCl	linear, $C_{\infty v}$, HCN···HCl	62 {mw: B_0, CD, χ(^{14}N), χ(Cl), χ(D), r(N···Cl)}; 63 {mw: μ}
	HBr	linear, $C_{\infty v}$, HCN···HBr	64 {mw: B_0, CD, χ(^{14}N), χ(Br), r(N···Br)}
	HCN	linear, $C_{\infty v}$, HCN···HCN	65 {IR: B_0, r(N···C)}; 24 {mw: B_0, r(N···C)}; 26 {mw: B_0, CD, χ(^{14}N), r(N···C)}; 66 {mw: B_0, CD, χ(D)}; 63 {mw: μ}; 25 {mw: B_0, B_v, CD, ν_σ, ν_β}
	HCF$_3$	C_{3v}, HCN···HCF$_3$	67 {mw: B_0, CD, χ(^{14}N), χ(D), r(N···C)}
CH$_3$CN	HF	C_{3v}, CH$_3$CN···HF	10 {IR: ν_S, ν_B, ν_σ, ν_β}; 18 {mw: B_0, B_v, CD, ν_β, ν_σ, r(N···F)}; 56 {mw: B_0, χ(^{14}N), χ(D), D^{HF}, r(N···F)}; 68 {mw: B_0, χ(^{14}N), D^{HF}, r(N···F)}; 57 {mw: CD}
	HCl	C_{3v}, CH$_3$CN···HCl	69 {IR: ν_S, ν_σ}
HCCCN	HF	linear, $C_{\infty v}$, HCCCN···HF	70 {mw and IR: B_0, B_v, CD, χ(^{14}N), ν_β, ν_S, ν_σ, r(N···F)}
NCCN	HF	linear, $C_{\infty v}$, NCCN···HF	48 {mw: B_0, CD, χ(^{14}N), D^{HF}, r(N···F)}
(CH$_3$)$_3$CCN	HF	C_{3v}, (CH$_3$)$_3$CCN···HF	71 {mw and IR: B_0, B_v, ν_β, r(N···F)}
NH$_3$	HF	C_{3v}, H$_3$N···HF	72 {mw: B_0, CD, χ(^{14}N), μ}
	HCN	C_{3v}, H$_3$N···HCN	65 {IR: B_0, r(N···C)}; 73 {mw: B_0, CD, χ(^{14}N), μ, r(N···C)}
	HCCH	C_{3v}, H$_3$N···HCCH	74 {mw: B_0, CD, χ(^{14}N), μ, r(N···C)}
N$_2$	HF	linear, $C_{\infty v}$, N$_2$···HF	47 {mw: B_0, CD, χ(^{14}N), D^{HF}, r(N···F)}; 38 {mw: B_0, CD, χ(D), D^{HF}}; 84 {mw: g, Q_m}
	HCl	linear, $C_{\infty v}$, N$_2$···HCl	51 {mw: B_0, CD, χ(^{14}N), χ(Cl), μ, r(N···Cl)}
	HCN	linear, $C_{\infty v}$, N$_2$···HCN	50 {mw: B_0, CD, χ(^{14}N), χ(D), r(N···C)}
PH$_3$	HF	C_{3v}, H$_3$P···HF	75 {mw: B_0, CD, χ(D), D^{HF}, r(P···F)}
	HCl	C_{3v}, H$_3$P···HCl	76 {mw: B_0, CD, χ(Cl), r(P···Cl)}
	HBr	C_{3v}, H$_3$P···HBr	77 {mw: B_0, CD, χ(Br), r(P···Br)}
	HCN	C_{3v}, H$_3$P···HCN	78 {mw: B_0, CD, χ(^{14}N), r(P···C)}; 79 {mw: μ}
P(CH$_3$)$_3$	HCN	C_{3v}, (CH$_3$)$_3$P···HCN	80 {mw: B_0, CD, χ(^{14}N), r(P···C)}
CO	HF	linear, $C_{\infty v}$, OC···HF	81 {mw: B_0, CD, r(C···F)}; 82 {mw: B_0, CD, χ(D), D^{HF}, r(N···F)}; 83 {mw: μ}; 84 {mw: g, Q_m}; 85 {IR: ν_S, B_v, r'(C···F)}
	HCl	linear, $C_{\infty v}$, OC···HCl	86 {mw: B_0, CD, χ(Cl), r(C···Cl)}; 87 {mw: μ}; 84 {mw: g, Q_m}
	HBr	linear, $C_{\infty v}$, OC···HBr	88 {mw: B_0, CD, χ(Br), r(C···Br)}
	HCN	linear, $C_{\infty v}$, OC···HCN	89 {mw: B_0, CD, χ(^{14}N), χ(D), r(C···C)}
CO$_2$	HF	linear, $C_{\infty v}$, OCO···HF	46 {mw: B_0, CD, χ(D), D^{HF}, μ, r(O···F)}; 90 {mw: g}
	HCl	linear, $C_{\infty v}$, OCO···HCl	91 {mw: B_0, CD, χ(Cl), χ(D), μ, r(O···Cl); 90 {mw: g}
	HCN	T-shaped, C_{2v}, $\overset{O}{\underset{O}{\overset{\|}{\underset{\|}{C}}}}$···NCH	92 {mw: B_0, CD, χ(^{14}N), μ, r(C···N)}
OCS	HF	linear, $C_{\infty v}$, SCO···HF	46 {mw: B_0, CD, D^{HF}, μ, r(O···F)}, 90 {mw: g}; 93 {mw: B_0, CD, χ(^{33}S), r(O···F)}
	HCl	linear, $C_{\infty v}$, SCO···HCl	94 {mw: B_0, CD, χ(Cl), r(O···Cl)}
Hg	HCl	linear, $C_{\infty v}$, Hg···HCl	95 {mw: B_0, CD, χ(Cl), χ(^{201}Hg), r(Hg···Cl)}
	HCN	linear, $C_{\infty v}$, Hg···HCN	95 {mw: χ(^{201}Hg)}
		B. Nonbonded Pair as Acceptor; Asymmetric Rotor Species	
H$_2$O	HF	C_S, pyramidal at O, H$_2$O···HF	96 {IR: ν_S, ν_B}; 33 {mw: B_0, CD, r(O···F)}; 20 {mw: B_0, B_v, CD, $\nu_{\beta(o)}$, $\nu_{\beta(i)}$, ν_σ, inversion P.E. function}; 34 {mw: B_0, B_v, CD, $\nu_{\beta(o)}$}; 97 {mw: B_v, P.E. function}; 32 {mw: μ_0, μ_v}, 98 {mw: B_0, χ_{aa}(D), D_{aa}^{HF}}
	HCl	Effectively planar, H$_2$O···HCl, probably C_S, pyramidal at O at equilibrium	99 {mw: B_0, CD, χ_{aa}(Cl), χ_{bb}(Cl), r(O···Cl)}
	HCN	Effectively planar, H$_2$O···HCN, probably C_S, pyramidal at O at equilibrium	100,101 {mw: B_0, CD, χ_{aa}(^{14}N), χ_{bb}(^{14}N), χ_{aa}(D), χ_{aa}(^{17}O), r(O···C)}
	HCCH	Effectively planar, H$_2$O···HCCH, probably, C_S, pyramidal at O at equilibrium	102 {mw: B_0, CD, μ_a, r(O···C)}
	H$_2$O	C_S, pyramidal arrangement around O on proton acceptor, H$_2$O···HOH	21,103,104,105 {mw: B_0, CD, μ_a, tunneling, r(O···O)}
CH$_3$OH	HF	Presumably, pyramidal at O, $\overset{H}{\underset{CH_3}{\diagdown}}$O···HF	106,107 {IR: ν_S, ν_σ, ν_B}
	HCl	C_1, pyramidal at O, $\overset{H}{\underset{CH_3}{\diagdown}}$O···HCl	108 {IR: ν_S}; 109 {mw: B_0, B_v, CD, χ_{aa}(Cl), χ_{bb}(Cl), r(O···Cl)}
(CH$_3$)$_2$O	HF	C_S, pyramidal at O, (CH$_3$)$_2$O···HF	15,16,107 {IR: ν_S, ν_σ, ν_β}; 110 {mw: B_0, r(O···F)}
	HCl	Presumably, as for (CH$_3$)$_2$O···HF	9,14,107 {IR: ν_S, ν_σ, ν_B, ν_β}
▷O	HF	C_S, pyramidal at O, ▷O···HF	44 {mw and IR: ν_S, B_0, CD, μ_a, r(O···F)}
	HCN	C_S, pyramidal at O, ▷C···HCN	111 {mw: B_0, B_v, CD, χ(^{14}N), r(O···C)}
◇O	HF	C_S, pyramidal at O, ◇O···HF	59 {mw and IR: ν_S, B_0, CD, r(O···F)}
▭O	HF	C_S, pyramidal at O, ▭O···HF	112 {mw: B_0, CD, r(O···F)}
▭O	HCl	C_{2v}, planar at O, ▭O···HCl	113 {mw: B_0, CD, χ_{aa}(Cl), χ_{bb}(Cl), r(O···Cl)}

TABLE XII (Continued)

proton acceptor, B	proton donor, HA	equilibrium geometry	ref {type of spectrum: derived properties}[a]
H_2CO	HF	C_S, planar trigonal at O, $H_2CO\cdots HF$	114 {mw: B_0, CD, $D_{aa}{}^{HF}$, μ_a, μ_b, $r(O\cdots F)$}
N_2O	HF	C_S, planar trigonal at O, $NNO\cdots HF$	45 {mw: B_0, μ_a, μ_b, $r(O\cdots F)$}
SO_2	HF, HCl	C_S, planar-cis, $OSO\cdots HX$	115 {mw: B_0, CD, $\chi_{aa}(Cl)$, $\chi_{bb}(Cl)$, $r(O\cdots X)$}
H_2S	HF	C_S, pyramidal at S, $H_2S\cdots HF$	43 {mw: B_0, CD, $D_{aa}{}^{HF}$, μ_a, μ_b, $r(S\cdots F)$}; 55 {mw: B_0, CD, $D_{aa}{}^{HF}$, $\chi_{aa}(D)$, $\chi_{aa}({}^{33}S)$}
	HCl	C_S, pyramidal at S, $H_2S\cdots HCl$	116 {mw: B_0, CD, $\chi_{aa}(Cl)$, $r(S\cdots Cl)$}
	HCN	C_S, pyramidal at S, $H_2S\cdots HCN$	117 {mw: B_0, CD, $\chi_{aa}({}^{14}N)$, $r(S\cdots C)$}
HF	HF	${}^{H}\diagdown_{F\cdots HF}$ effectively C_S	22,118 {mw: B_0, CD, μ_a, $\chi_{aa}(D)$, tunneling, $r(F\cdots F)$}; 29,119 {IR: ν_S-rotation-tunneling fine structure}
	HCl	Presumably ${}^{H}\diagdown_{F\cdots HCl}$	42 {mw: B_0, CD, $\chi_{aa}(Cl)$, μ_a, $r(F\cdots Cl)$}
HCl	HCl	Probably as for $(HF)_2$	120 {IR: ν_S, B_0, B_v, tunneling, r_{cm}}

C. π-Bond Pair as Acceptor; Asymmetric Rotor Species

proton acceptor, B	proton donor, HA	equilibrium geometry	ref {type of spectrum: derived properties}[a]
$HC\equiv CH$	HF	C_{2v}, planar, T-shaped, (HC≡CH···HF)	121 {mw: B_0, $D_{aa}{}^{HF}$, $\chi_{aa}(D)$, $r(\text{center}\cdots F)$}[b]
	HCl	C_{2v}, planar, T-shaped, (HC≡CH···HCl)	122 {mw: B_0, CD, $\chi_{aa}(Cl)$, $\chi_{bb}(Cl)$, $r(\text{center}\cdots Cl)$}; 123 {mw: $\chi_{aa}(D)$, $\chi_{bb}(D)$}
	HCN	C_{2v}, planar, T-shaped, (HC≡CH···HCN)	124 {mw: B_0, CD, $\chi_{aa}({}^{14}N)$, $\chi_{bb}({}^{14}N)$, $\chi_{aa}(D)$, $\chi_{bb}(D)$, $r(\text{center}\cdots C)$}
$CH_3C\equiv CH$	HF	T-shaped, heavy atoms planar, (similar to acetylene···HF)	125 {mw: B_0, $D_{aa}{}^{HF}$, $\chi_{aa}(D)$, potential barrier}
$H_2C=CH_2$	HF	C_{2v}, HF perpendicular to plane of $CH_2=CH_2$; (CH₂=CH₂···HF)	40 {mw: B_0, $D_{aa}{}^{HF}$, $\chi_{aa}(D)$, $r(\text{center}\cdots F)$}
	HCl	C_{2v}, HCl perpendicular to $CH_2=CH_2$ plane; (CH₂=CH₂···HCl)	126 {mw: B_0, CD, $\chi_{aa}(Cl)$, $\chi_{bb}(Cl)$, $r(\text{center}\cdots Cl)$}; 123 {mw: $\chi_{aa}(D)$, $\chi_{bb}(D)$}; 127 {mw: g, Q_m}
	HCN	C_{2v}, HCN perpendicular to $CH_2=CH_2$ plane; (CH₂=CH₂···HCN)	128 {mw: B_0, CD, $\chi_{aa}({}^{14}N)$, $\chi_{bb}({}^{14}N)$, $\chi_{aa}(D)$, $r(\text{center}\cdots C)$}
◁	HF	C_{2v}, HF lies along median of cyclopropane triangle, ◁···HF	129 {mw: B_0, CD, $D_{aa}{}^{HF}$, $\chi_{aa}(D)$, $r(\text{center}\cdots F)$}
	HCl	C_{2v}, HCl lies along median of cyclopropane triangle, ◁···HCl	130,131 {mw: B_0, CD, $\chi_{aa}(Cl)$, $\chi_{bb}(Cl)$, $r(\text{center}\cdots Cl)$}
	HCN	C_{2v}, HCN lies along median of cyclopropane triangle, ◁···HCN	132 {mw: B_0, CD, $\chi_{aa}({}^{14}N)$, $\chi_{bb}({}^{14}N)$, $r(\text{center}\cdots C)$}
⬡	HF	C_{6v}, HF lies along C_6 axis of benzene, with H closer to ring than F	133 {mw: B_0, CD, $\chi(D)$, μ, $r(\text{center}\cdots F)$}
	HCl	C_{6v}, HCl lies along C_6 axis of benzene, with H closer to ring than Cl	134 {mw: B_0, CD, $\chi(Cl)$, $r(\text{center}\cdots Cl)$}

[a] The reference number is followed in parentheses by the abbreviation mw or IR to indicate the type of spectrum reported in that reference. The abbreviation is then followed by a list of the principal spectroscopic quantities derived from the spectrum. B_0 is used to indicate the appropriate set of ground-state rotational constants; B_v is used when rotational constants associated with at least one vibrationally excited state have been determined; CD indicates that centrifugal distortion constants are available; $\chi(A)$ indicates a nuclear quadrupole coupling constant associated with nucleus A; D^{HF} indicates that an HF nuclear spin–nuclear spin coupling constant is available; g and Q_m are g-factors and electric quadrupole moments, respectively, from the Zeeman effect; $r(B\cdots A)$ is an internuclear distance between the dimer components and is used to indicate that geometrical conclusions are available; ν_S, ν_σ, ν_B, and ν_β mean that vibrational separations in the indicated mode have been determined; D_e is an equilibrium dissociation energy for $B\cdots HA = B + HA$; and μ is an electric dipole moment. [b] $r(\text{center}\cdots A)$ is the distance from the center of a π-bond or the center of a C–C bond in cyclopropane or the center of the benzene ring to the appropriate heavy atom of HA.

where μ is defined in eq 13. Hence, D_0 follows once the $n_{0,0}$ are known. We show in Table XI a typical set of $n_{0,0}$ and D_0 values from an experiment[19,37] involving an equilibrium mixture of HCN,HF, and HCN···HF measured at $T = 190$ K. The average of a number of such measurements is $D_0 = 18.9 \pm 1.1$ kJ mol^{-1}, which on correction for the known zero-point contribution according to

$$D_e = D_0 + L\sum_i \tfrac{1}{2}h\nu_i(B\cdots HA) - L\sum_i \tfrac{1}{2}h\nu_i(B) - L\sum_i \tfrac{1}{2}h\nu_i(HA) \quad (25)$$

leads to the equilibrium dissociation energy $D_e = 26.1$

± 1.6 kJ mol^{-1}. This is the only value of D_e so far determined by rotational spectroscopy.

V. Summary and Generalizations

We have shown in this article how a wide range of properties of hydrogen-bonded dimers can be determined from investigations of their vibrational and rotational spectra. These properties include the dimer geometry, the internal dynamics of the subunits, details of the potential energy function, and changes in the electrical and geometrical nature of the components on formation of the hydrogen bond. We have discussed how the properties follow from the spectroscopic ob-

servations by reference mainly to the heterodimer HCN···HF. In fact, similar investigations, although less complete, have been made for a number of dimers B···HA.

A summary of the hydrogen-bonded dimers B···HA investigated by rotational and vibrational spectroscopies, which includes numerous other dimers[62–134] besides those already mentioned in the text, is given in Table XII. We have excluded from the table the cases where B is a rare gas atom because these are not usually viewed as hydrogen-bonded species and have been extensively discussed previously. Many low-resolution investigations of hydrogen-bonded dimers by infrared spectroscopy have been made in the gas phase and these have been reviewed elsewhere.[5] Such investigations are referred to in Table XII only when the rotational spectrum of the species has also been investigated or the species is particularly simple or important. The limited number of high-resolution infrared studies of B···HX are included in Table XII. For each entry in Table XII, we give the proton acceptor, the proton donor, the equilibrium geometry of the dimer (when known), and appropriate references to papers listed at the end of the article. Each reference number in Table XII is followed in parenthesis by symbols indicating the type of spectroscopy employed and the principal spectroscopic quantities determined in the investigation. The meanings of the symbols are discussed in the footnotes to the table. Of course, molecular properties are also, in general, determined from the spectroscopic constants in the cited papers. The types of molecular properties available will be clear from the discussion in section III and the cited literature should be referred to for details.

As a result of the investigations referred to in Table XII, three important generalizations about the hydrogen bond (already mentioned in this article) have emerged. The first concerns the lengthening of the H–F bond on formation of dimers B···HF. It has been found (see Figure 19 in section IVC) that the lengthening δr increases smoothly and almost linearly as the strength of the hydrogen bond (as measured by the force constant, k_σ) increases.[39] The second generalization refers to the quadratic force constants for bending the hydrogen-bonded dimer. It has been shown in the few cases investigated so far[18,19,58] that bending at the H atom in B···HF is more strongly resisted than bending at the binding atom of B.

The third generalization refers to the directional character of the hydrogen bond and has led to a set of rules[135] which allows the shapes of a large number of hydrogen-bonded dimers to be rationalized in terms of nonbonding and π-bonding electron pairs on B. The rules are set out below.

The gas-phase geometry of a dimer B···HX can be obtained in terms of the nonbonding and π-bonding electron pairs on B as follows: (i) the axis of the HX molecule coincides with the supposed axis of a nonbonding pair as conventionally envisaged, or, if B has no nonbonding electron pairs but has π-bonding pairs, (ii) the axis of the HX molecule intersects the internuclear axis of the atoms forming the π-bond and is perpendicular to the plane of symmetry of the π-orbital. Rule (i) is definitive when B has both nonbonding and π-bonding pairs.

Since these rules were enunciated, a number of further examples consistent with them has been reported, notably H_2S···HF[43,55] and H_2CO···HF.[114] For the former, the angle ϕ, defined in the same way as for H_2O···HF, is found to be very close to 90° in accord with the simple model of H_2S which places a lone pair in a p orbital at right angles to the H_2S plane. In H_2CO···HF, the angle CO···F is found to be 110° which again is readily rationalized on the basis of a trigonal environment for the O atom. The deviation from the trigonal angle 120° is readily understood in terms of the valence-shell–electron-pair repulsion model, as discussed by Gillespie and Nyholm.[136] Nevertheless, exceptions to the rules do exist, especially OCO···HX and SCO···HX where X = F,[46,93] Cl[91,94] and CN.[92] Thus when X = F and Cl, the dimers have the linear geometry indicated. These results will be discussed further below but it can be noted straightaway that the intermolecular stretching force constants for these dimers are comparable with those of van der Waals complexes, rather than with those of generally recognized hydrogen-bonded dimers. Indeed, for X = CN the dimer is clearly not hydrogen bonded[92] since it has a T-shaped geometry with the N atom of HCN facing the C atom of CO_2.

A quantitative counterpart of the lone-pair model has been developed by Buckingham and Fowler[137,138] for predicting geometries of dimers. This quantitative electrostatic model is kept computationally simple by replacing the charge density of any particular monomer, as obtained from accurate ab initio calculations, by point multipoles—charges, dipoles, and quadrupoles—located on each atom and in some cases at bond midpoints. These multipoles are embedded in hard van der Waals spheres which represent the short range repulsion and determine the hydrogen bond length at which the electrostatic interaction energy between the sets of distributed multipoles representing each monomer is to be determined. In almost all cases where an experimental structure is known this electrostatic model proves qualitatively and often quantitatively correct.

The validity of the model has been examined by SCF calculations for a number of dimers,[139] using Morokuma[140] analysis, which lead to results that are consistent with an electrostatic model. More recently strong support for the Buckingham-Fowler model has been obtained by a comparison of its predictions with the results of ab initio calculations[141] for a number of carefully chosen dimers. The calculated interaction energy is partitioned into electrostatic, exchange, polarization, and charge transfer contributions. The results of the calculations show that the electrostatic contribution is generally the dominant factor determining both the strength and directionality of the complex, and that the angular dependence of the electrostatic contribution parallels that obtained from the point multipole model. Where steric effects are important, as in CO_2···H_2O, or where the angular dependence of the electrostatic term is weak, as in C-O_2···HF, the geometry may be influenced by other factors and the geometric predictions of the model may be less reliable. Such cases are relatively few and the conditions under which they arise have been examined.[141] In summary the ab initio calculations lead to quantitative geometries for which the dominant determining factor is the electrostatic interaction energy.

The distributed moment model[137,138] provides a valuable approximation both qualitatively and quantitatively within limits now explored, and has the advantage that the computation is kept relatively simple. The lone-pair approach[135] can be seen as an easily applied qualitative electrostatic model of hydrogen-bonding interactions.

An alternative approach based on the HOMO/LUMO method has been put forward by Klemperer[142] and co-workers. In the model, as described by Dyke:[8] "...the hydrogen bond is viewed as an electron donor-acceptor complex in which a pair of electrons from the highest occupied molecular orbital of the Lewis base is donated to the lowest unoccupied molecular orbital of the Lewis acid. If the donor electron pair is assumed to have the appropriate hybridization, and the acceptor orbital to be axially symmetric, the above structures can be rationalized as giving maximal overlap between the HOMO and LUMO."

The generalizations discussed above have important implications for hydrogen bonding in condensed phases. Thus the finding that bending of a hydrogen bond at the heavy atom is relatively easy to bring about while bending at the hydrogen atom is more strongly resisted is directly relevant to understanding distortions from lone-pair geometries in the liquid and solid states. Distortions from the lone-pair axis can readily occur at the demand of the hydrogen-bond environment while distortions leading to bent hydrogen bonds are energetically much less probable. For the case of hydrogen bonds to oxygen these arguments can be taken a stage further. For $H_2O \cdots HF$ it is found that distortion out of the plane is much less demanding energetically than the corresponding in plane distortion.[58] The result is consistent with statistical analyses of large numbers of X-ray diffraction[143] and neutron diffraction[144] investigations of O–H$\cdots$O bonds. Both statistical studies lead to the conclusion that while there is some preference for hydrogen bonding within or near the plane containing the lone-pair axes, there is no distinct preference for hydrogen bond formation within that plane. The conclusions are just those to be expected if the potential energy functions of O$\cdots$H–O hydrogen bonds are of the same form as those for O$\cdots$H–F.[58] Finally, both the X-ray[143] and the neutron[144] diffraction statistical analyses show that, when proper account is taken of weighting, hydrogen bonds bent by more than about 15° are exceptional in these systems, which is entirely consistent with expectations outlined above.

There are some important areas of vibrational spectroscopy of hydrogen-bonded dimers which have been discussed recently but which demand to be mentioned here. The first is the phenomenon of vibrational predissociation which provides additional information about the intermolecular potential energy function of the dimer and has been reviewed in detail elsewhere.[145] The second concerns vibrational Raman spectra of hydrogen-bonded species using the CARS technique applied to pulsed molecular beams.[146] The third is the field of matrix isolation studies, as reviewed[147] by Andrews and by Barnes.

Finally it is noted that while this review has been concerned with electronic ground states of simple hydrogen bonded dimers having a single hydrogen bond, recent investigations by Tomoda and Kimura of the photoelectron spectroscopy of the gas-phase $(H_2O)_2$

dimer have opened up the possibility of exploring the properties of electronically excited states of such dimers.[148,149]

VI. References

(1) Latimer, W. M.; Rodebush, W. H. *J. Am. Chem. Soc.* **1920**, *42*, 1419.
(2) Schuster, P.; Zundel, G.; Sandorfy, C. *The Hydrogen Bond*; North Holland: Amsterdam, 1976; Vols. I, II, and III.
(3) Legon, A. C. *J. Phys. Chem.* **1983**, *87*, 2064.
(4) Legon, A. C. *Annu. Rev. Phys. Chem.* **1983**, *34*, 275.
(5) Millen, D. J. *J. Mol. Struct.* **1983**, *100*, 351.
(6) Millen, D. J. *J. Mol. Struct.* **1984**, *113*, 227.
(7) Sandorfy, C. *Top. Curr. Chem.* **1984**, *120*, 41.
(8) Dyke, T. R. *Top. Curr. Chem.* **1984**, *120*, 85.
(9) Bertie, J. E.; Millen, D. J. *J. Chem. Soc.* **1965**, 497.
(10) Thomas, R. K. *Proc. R. Soc. London, A* **1971**, *325*, 133.
(11) Millen, D. J.; Schrems, O. *Chem. Phys. Lett.* **1983**, *101*, 320.
(12) Bevan, J. W.; Martineau, B.; Sandorfy, C. *Can. J. Chem.* **1979**, *57*, 1341.
(13) (a) Kyrö, E.; Warren, R.; McMillan, K.; Eliades, M.; Danzeiser, D.; Shoda-Chaghervand, P.; Lieb, S. G.; Bevan, J. W. *J. Chem. Phys.* **1983**, *78*, 5881. (b) Bevan, J. W., to be published.
(14) Bertie, J. E.; Falk, M. V. *Can. J. Chem.* **1973**, *51*, 1713.
(15) Arnold, J.; Millen, D. J. *J. Chem. Soc.* **1965**, 503.
(16) Thomas, R. K. *Proc. R. Soc. London, A* **1971**, *322*, 137.
(17) Bevan, J. W.; Legon, A. C.; Millen, D. J.; Rogers, S. C. *J. Chem. Soc., Chem. Commun.* **1975**, 130.
(18) Bevan, J. W.; Legon, A. C.; Millen, D. J.; Rogers, S. C. *Proc. R. Soc. London, A* **1980**, *370*, 239.
(19) Legon, A. C.; Millen, D. J.; Rogers, S. C. *Proc. R. Soc. London, A* **1980**, *370*, 213.
(20) Kisiel, Z.; Legon, A. C.; Millen, D. J. *Proc. R. Soc. London, A* **1982**, *381*, 419.
(21) Dyke, T. R.; Mack, K. M.; Muenter, J. S. *J. Chem. Phys.* **1977**, *66*, 498.
(22) Dyke, T. R.; Howard, B. J.; Klemperer, W. *J. Chem. Phys.* **1972**, *56*, 2442.
(23) Balle, T. J.; Flygare, W. H. *Rev. Sci. Instrum.* **1981**, *52*, 33.
(24) Legon, A. C.; Millen, D. J.; Mjöberg, P. *J. Chem. Phys. Lett.* **1977**, *47*, 589.
(25) Georgiou, K.; Legon, A. C.; Millen, D. J.; Mjöberg, P. *J. Proc. R. Soc. London, A* **1985**, *399*, 377.
(26) Campbell, E. J.; Buxton, L. W.; Flygare, W. H. *Chem. Phys.* **1981**, *56*, 399.
(27) Legon, A. C.; Millen, D. J.; Willoughby, L. C. *Proc. R. Soc. London, A* **1985**, *401*, 327.
(28) Sheppard, N. In *Hydrogen Bonding*; Hadzi, D. Ed.; Pergamon: London, 1959; p 85.
(29) Pine, A. S.; Lafferty, W. J. *J. Chem. Phys.* **1983**, *78*, 2154.
(30) Dyke, T. R.; Muenter, J. S. In *International Review Science: Physical Chemistry Series Two*; Buckingham, A. D., Ed.; Butterworths: London 1975; Vol. 2.
(31) Townes, C. H.; Schawlow, A. L. *Microwave Spectroscopy*; McGraw-Hill: New York, 1955.
(32) Kisiel, Z.; Legon, A. C.; Millen, D. J. *J. Chem. Phys.* **1983**, *78*, 2910.
(33) Bevan, J. W.; Kisiel, Z.; Legon, A. C.; Millen, D. J.; Rogers, S. C. *Proc. R. Soc. London, A* **1980**, *372*, 441.
(34) Cazzoli, G.; Favero, P. G.; Lister, D. G.; Legon, A. C.; Millen, D. J.; Kisiel, Z. *Chem. Phys. Lett.* **1985**, *117*, 543.
(35) Legon, A. C.; Millen, D. J.; Rogers, S. C. *Chem. Phys. Lett.* **1976**, *41*, 137.
(36) Legon, A. C.; Millen, D. J.; Rogers, S. C. *J. Mol. Spectrosc.* **1978**, *70*, 209.
(37) Legon, A. C.; Millen, D. J.; Mjöberg, P. J.; Rogers, S. C. *Chem. Phys. Lett.* **1978**, *55*, 157.
(38) Legon, A. C.; Willoughby, L. C. *Chem. Phys. Lett.* **1984**, *109*, 502.
(39) Legon, A. C.; Millen, D. J. *Proc. R. Soc. London, A* **1986**, *404*, 89.
(40) Shea, J. A.; Flygare, W. H. *J. Chem. Phys.* **1982**, *76*, 4857.

(41) Barfield, M.; Gottleib, A. P. W.; Doddrell, D. M. *J. Chem. Phys.* 1978, *69*, 4504.

(42) Janda, K. C.; Steed, J. M.; Novick, S. E.; Klemperer, W. *J. Chem. Phys.* 1977, *67*, 5167.

(43) Viswanathan, R.; Dyke, T. R. *J. Chem. Phys.* 1982, *77*, 1166.

(44) Georgiou, A. S.; Legon, A. C.; Millen, D. J. *Proc. R. Soc. London, A* 1981, *372*, 511.

(45) Joyner, C. H.; Dixon, T. A.; Baiocchi, F. A.; Klemperer, W. *J. Chem. Phys.* 1981, *74*, 6550.

(46) Baiocchi, F. A.; Dixon, T. A.; Joyner, C. H.; Klemperer, W. *J. Chem. Phys.* 1981, *74*, 6544.

(47) Soper, P. D.; Legon, A. C.; Read, W. G.; Flygare, W. H. *J. Chem. Phys.* 1982, *76*, 292.

(48) Legon, A. C.; Soper, P. D.; Flygare, W. H. *J. Chem. Phys.* 1981, *74*, 4936.

(49) Keenan, M. R.; Buxton, L. W.; Campbell, E. J.; Balle, T. J.; Flygare, W. H. *J. Chem. Phys.* 1980, *73*, 3523.

(50) Goodwin, E. J.; Legon, A. C. *J. Chem. Phys.* 1985, *82*, 4434.

(51) Altman, R. S.; Marshall, M. D.; Klemperer, W. *J. Chem. Phys.* 1983, *79*, 57.

(52) Millen, D. J. *Can. J. Chem.* 1985, *63*, 1477.

(53) Dixon, T. A.; Joyner, C. H.; Baiocchi, F. A.; Klemperer, W. *J. Chem. Phys.* 1981, *74*, 6539.

(54) Legon, A. C.; Soper, P. D.; Flygare, W. H. *J. Chem. Phys.* 1981, *74*, 4944.

(55) Willoughby, L. C.; Fillery-Travis, A. J.; Legon, A. C. *J. Chem. Phys.* 1984, *81*, 20.

(56) Cope, P.; Legon, A. C.; Millen, D. J.; Willoughby, L. C. *J. Chem. Soc. Faraday Trans. 2*, to be published.

(57) Legon, A. C.; Millen, D. J.; Rogers, S. C. *J. Mol. Struct.* 1980, *67*, 29.

(58) Kisiel, Z.; Legon, A. C.; Millen, D. J. *J. Mol. Struct.* 1984, *112*, 1.

(59) Georgiou, A. S.; Legon, A. C.; Millen, D. J. *J. Mol. Struct.* 1980, *69*, 69.

(60) Legon, A. C.; Millen, D. J.; North, H. M., unpublished observations.

(61) Cope, P.; Legon, A. C.; Millen, D. J. *J. Chem. Soc., Faraday Trans. 2*, to be published.

(62) Legon, A. C.; Campbell, E. J.; Flygare, W. H. *J. Chem. Phys.* 1982, *76*, 2267.

(63) Campbell, E. J.; Kukolich, S. G. *Chem. Phys.* 1983, *76*, 225.

(64) Campbell, E. J.; Legon, A. C.; Flygare, W. H. *J. Chem. Phys.* 1983, *78*, 3494.

(65) Jones, W. J.; Seel, R. M.; Sheppard, N. *Spectrochim. Acta* 1969, *25A*, 385.

(66) Fillery-Travis, A. J.; Legon, A. C.; Willoughby, L. C.; Buckingham, A. D. *Chem. Phys. Lett.* 1983, *102*, 126.

(67) Goodwin, E. J.; Legon, A. C. *J. Chem. Phys.* 1986, *84*, 1988.

(68) Soper, P. D.; Legon, A. C.; Read, W. G.; Flygare, W. H. *J. Phys. Chem.* 1981, *85*, 3440.

(69) Thomas, R. K.; Thompson, H. W. *Proc. R. Soc. London, A* 1970, *316*, 303.

(70) Georgiou, K.; Legon, A. C.; Millen, D. J.; North, H. M.; Willoughby, L. C. *Proc. R. Soc. London, A* 1984, *394*, 387.

(71) Georgiou, A. S.; Legon, A. C.; Millen, D. J. *Proc. R. Soc. London, A* 1980, *370*, 257.

(72) Howard, B. J.; Langridge-Smith, P. R. R., to be published.

(73) Fraser, G. T.; Leopold, K. R.; Nelson, D. D., Jr.; Tung, A.; Klemperer, W. *J. Chem. Phys.* 1984, *80*, 3073.

(74) Fraser, G. T.; Keopold, K. R.; Klemperer, W. *J. Chem. Phys.* 1984, *80*, 1423.

(75) Legon, A. C.; Willoughby, L. C. *Chem. Phys.* 1983, *74*, 127.

(76) Legon, A. C.; Willoughby, L. C. *J. Chem. Soc., Chem. Commun.* 1982, 997.

(77) Willoughby, L. C.; Legon, A. C. *J. Phys. Chem.* 1983, *87*, 2085.

(78) Legon, A. C.; Willoughby, L. C. *Chem. Phys.* 1984, *85*, 443.

(79) Legon, A. C.; Willoughby, L. C. *Chem. Phys. Lett.* 1984, *111*, 566.

(80) Hirani, H. L.; Legon, A. C.; Millen, D. J.; Willoughby, L. C. *J. Mol. Struct.* 1984, *125*, 171.

(81) Legon, A. C.; Soper, P. D.; Keenan, M. R.; Minton, T. K.; Balle, T. J.; Flygare, W. H. *J. Chem. Phys.* 1980, *73*, 583.

(82) Legon, A. C.; Soper, P. D.; Flygare, W. H. *J. Chem. Phys.* 1981, *74*, 4944.

(83) Campbell, E. J.; Read, W. G.; Shea, J. A. *Chem. Phys. Lett.* 1983, *94*, 69.

(84) Read, W. G.; Campbell, E. J. *J. Chem. Phys.* 1983, *78*, 6515.

(85) Kyrö, E. K.; Shoja-Chaghervand, P.; McMillan, K.; Eliades, M.; Danzeiser, D.; Bevan, J. W. *J. Chem. Phys.* 1983, *79*, 78.

(86) Soper, P. D.; Legon, A. C.; Flygare, W. H. *J. Chem. Phys.* 1981, *74*, 2138.

(87) Altman, R. S.; Marshall, M. D.; Klemperer, W.; Krupnov, A. *J. Chem. Phys.* 1983, *79*, 52.

(88) Keenan, M. R.; Minton, T. K.; Legon, A. C.; Balle, T. J.; Flygare, W. H. *Proc. Natl. Acad. Sci. U.S.A.* 1980, *77*, 5583.

(89) Goodwin, E. J.; Legon, A. C. *Chem. Phys.* 1984, *87*, 81.

(90) Campbell, E. J.; Shea, J. A. *J. Chem. Phys.* 1983, *79*, 4082.

(91) Altman, R. S.; Marshall, M. D.; Klemperer, W. *J. Chem. Phys.* 1982, *77*, 4344.

(92) Leopold, K. R.; Fraser, G. T.; Klemperer, W. *J. Chem. Phys.* 1984, *80*, 1039.

(93) Legon, A. C.; Willoughby, L. C. *J. Mol. Struct.* 1985, *131*, 159.

(94) Goodwin, E. J.; Legon, A. C. *J. Chem. Soc. Faraday Trans. 2* 1985, *81*, 1709.

(95) Shea, J. A.; Campbell, E. J. *J. Chem. Phys.* 1984, *81*, 5326.

(96) Thomas, R. K. *Proc. R. Soc. London, A* 1975, *344*, 579.

(97) Kisiel, Z.; Legon, A. C.; Millen, D. J. *J. Mol. Structure* 1985, *131*, 201.

(98) Legon, A. C.; Willoughby, L. C. *Chem. Phys. Lett.* 1982, *92*, 333.

(99) Legon, A. C.; Willoughby, L. C. *Chem. Phys. Lett.* 1983, *95*, 449.

(100) Fillery-Travis, A. J.; Legon, A. C.; Willoughby, L. C. *Chem. Phys. Lett.* 1983, *98*, 369.

(101) Fillery-Travis, A. J.; Legon, A. C.; Willoughby, L. C. *Proc. R. Soc. London, A* 1984, *396*, 405.

(102) Petersen, K. I.; Klemperer, W. *J. Chem.Phys.* 1984, *81*, 3842.

(103) Dyke, T. R.; Muenter, J. S. *J. Chem. Phys.* 1974, *60*, 2929.

(104) Dyke, T. R. *J. Chem. Phys.* 1977, *66*, 492.

(105) Odutola, J. A.; Dyke, T. R. *J. Chem. Phys.* 1980, *72*, 5062.

(106) Schrems, O.; Legon, A. C.; Millen, D. J. *J. Chem. Soc., Faraday Trans. 2* 1975, *75*, 592.

(107) Couzi, M.; Le Calve, J.; Huong, P. V.; Lascombe, J. *J. Mol. Struct.* 1970, *5*, 363.

(108) Luck, W. A. P.; Schrems, O. *Chem. Phys. Lett.* 1980, *76*, 75.

(109) Cope, P.; Legon, A. C.; Millen, D. J. *Chem. Phys. Lett.* 1984, *112*, 59.

(110) Kisiel, Z.; Legon, A. C.; Millen, D. J.; North, H. M., to be published.

(111) Goodwin, E. J.; Legon, A. C.; Millen, D. J. *J. Chem. Phys.*, to be published.

(112) Collins, R. A.; Legon, A. C.; Millen, D. J., to be published.

(113) Shea, J. A.; Kukolich, S. G. *J. Chem. Phys.* 1983, *78*, 3545.

(114) Baiocchi, F. A.; Klemperer, W. *J. Chem. Phys.* 1983, *78*, 3509.

(115) Fillery-Travis, A. J.; Legon, A. C. *Chem. Phys. Lett.*, to be published.

(116) Goodwin, E. J.; Legon, A. C. *J. Chem. Soc., Faraday Trans. 2* 1984, *80*, 51.

(117) Goodwin, E. J.; Legon, A. C. *J. Chem. Soc., Faraday Trans. 2* 1984, *80*, 1669.

(118) Howard, B. J.; Dyke, T. R.; Klemperer, W. *J. Chem. Phys.* 1984, *81*, 5417.

(119) Pine, A. S.; Lafferty, W. J.; Howard, B. J. *J. Chem. Phys.* 1984, *81*, 2939.

(120) Ohashi, N.; Pine, A. S. *J. Chem. Phys.* 1984, *81*, 73.

(121) Read, W. G.; Flygare, W. H. *J. Chem. Phys.* 1982, *76*, 2238.

(122) Legon, A. C.; Aldrich, P. D.; Flygare, W. H. *J. Chem. Phys.* 1981, *75*, 625.

(123) Aldrich, P. D.; Campbell, E. J. *Chem. Phys. Lett.* 1982, *93*, 355.

(124) Aldrich, P. D.; Kukolich, S. G.; Campbell, E. J. *J. Chem. Phys.* 1983, *78*, 3521.

(125) Shea, J. A.; Bumgarner, R. E.; Henderson, G. *J. Chem. Phys.* 1984, *80*, 4605.

(126) Aldrich, P. D.; Legon, A. C.; Flygare, W. H. *J. Chem. Phys.* 1981, *75*, 2126.

(127) Kukolich, S. G.; Aldrich, P. D.; Read, W. G.; Campbell, E. J. *J. Chem. Phys.* 1983, *79*, 1105.

(128) Kukolich, S. G.; Read, W. G.; Aldrich, P. D. *J. Chem. Phys.* 1983, *78*, 3552.

(129) Buxton, L. W.; Aldrich, P. D.; Shea, J. A.; Legon, A. C.; Flygare, W. H. *J. Chem. Phys.* 1981, *75*, 2681.

(130) Legon, A. C.; Aldrich, P. D.; Flygare, W. H. *J. Am. Chem. Soc.* 1980, *102*, 7584.

(131) Legon, A. C.; Aldrich, P. D.; Flygare, W. H. *J. Am. Chem. Soc.* 1982, *104*, 1486.

(132) Kukolich, S. G. *J. Chem. Phys.* 1983, *78*, 4832.

(133) Baiocchi, F. A.; Williams, J. H.; Klemperer, W. *J. Phys. Chem.* 1983, *87*, 2079.

(134) Read, W. G.; Campbell, E. J.; Henderson, G. *J. Chem. Phys.* 1983, *78*, 3501.

(135) Legon, A. C.; Millen, D. J. *Faraday Discuss. Chem. Soc.* 1982, *73*, 71.

(136) Gillespie, R. J.; Nyholm, R. S. *Q. Rev., Chem. Soc.* 1957, *11*, 339.

(137) Buckingham, A. D.; Fowler, P. W. *J. Chem. Phys.* 1983, *79*, 6426.

(138) Buckingham, A. D.; Fowler, P. W. *Can. J. Chem.* 1985, *63*, 2018.

(139) Rendell, A. P. L.; Bacskay, G. B.; Hush, N. S. *Chem. Phys. Lett.* 1985, *117*, 400.

(140) Kitaura, K.; Morokuma, K. *Int. J. Quantum Chem.* 1976, *10*, 325.

(141) Hurst, G. J. B.; Fowler, P. W.; Stone, A. J.; Buckingham, A. D. *Int. J. Quantum Chem.*, to be published.
(142) Baiocchi, F. A.; Reiher, W.; Klemperer, W. *J. Chem. Phys.* **1983**, *79*, 6428.
(143) Kroon, J.; Kanters, J. A.; van Duijneveldt de Rijdt, J. G. C. M.; van Duijneveldt, F. B.; Vleigenthart, J. A. *J. Mol. Struct.* **1975**, *24*, 109.
(144) Cenarelli, C.; Jeffrey, G. A.; Taylor, R. *J. Mol. Struct.* **1981**, *70*, 255.

(145) Janda, K. C. *Adv. Chem. Phys.* **1985**, *60*, 201.
(146) Hopkins, G. A.; Maroncelli, M.; Nibler, J. W.; Dyke, T. R. *Chem. Phys. Lett.* **1985**, *114*, 97.
(147) Andrews, L. *J. Phys. Chem.* **1984**, *88*, 2940. Barnes, A. J. *J. Mol. Struct.* **1983**, *100*, 259.
(148) Tomoda, S.; Achiba, Y.; Kimura, K. *Chem. Phys. Lett.* **1982**, *87*, 197.
(149) Tomoda, S.; Kimura, K. *Chem. Phys. Lett.* **1984**, *111*, 434.